Санкт-Петербургский государственный университет

Институт химии

Дополнительные материалы к курсу «Магнитный резонанс»

на английском языке

Санкт-Петербург

2015 г.

Составитель:
к.ф.-м.н. П. М. Толстой

Рецензенты:
Рецензент 1, рецензент 2

Утверждено Ученым Советом Института химии СПбГУ в качестве учебного пособия для студентов 5-го и 6-го курса Института химии СПбГУ.

Оглавление

Введение

Данные методические материалы представляют собой краткое изложение основ спектроскопии ядерного магнитного резонанса на английском языке с приведением формул и математических выкладок, призванных помочь студентам в более глубоком освоении материала курса «Магнитный резонанс». Последовательность изложения соответствует программе курса и содержит часть иллюстративного материала из лекций. Объем материала, в особенности в том, что касается математических формул, превышает объем, даваемый на лекциях, и предназначен в первую очередь для студентов, жалеющих глубже разобраться в физических основах спектроскопии ЯМР.

1. Physical background of nuclear magnetic resonance

1.1. Classical description of magnetic dipole

1.1.1. Classical angular momentum

In classical physics an *angular momentum* of a rotating object is the measure of the extent to which it would preserve its state of rotation when acted upon by external torque. Angular momentum $\vec{I}$ of a rotating particle is defined as

$$\vec{I} = \vec{r} \times m\vec{V}, \tag{1.1}$$

where $\vec{r}$ is the distance to the axis of rotation, m is the mass of the particle and $\vec{V}$ is its linear velocity. Unit of angular momentum is N·m·s (kg·m^2·s^{-1}). Angular momentum is a vector directed by the right hand grip rule:

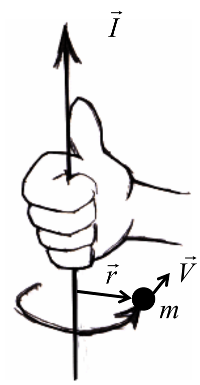

Figure 1.1. Right hand grip rule for the angular momentum.

Torque is defined as

$$\vec{D} = \vec{r} \times \vec{F}, \tag{1.2}$$

where $\vec{r}$ is the distance to the rotation point and $\vec{F}$ is the acting force. *Torque* is the measure of the extent to which force is able to change the angular momentum. Unit of torque is N·m (kg·m^2·s^{-2}), which technically coincides with the energy unit Joule but should not be interchanged with it, because torque is a vector and energy is a scalar. From equations (1.1) and (1.2) one can derive that torque is equal to the rate of change of angular momentum:

$$\vec{D} = \frac{d\vec{I}}{dt}. \tag{1.3}$$

From equations (1.1)-(1.3) it follows that if the force is perpendicular to rotational axis of a body then the angular momentum of the body starts to rotate in the plane perpendicular to the force (see Figure 1.2). Rate of this new rotation is proportional to the torque.

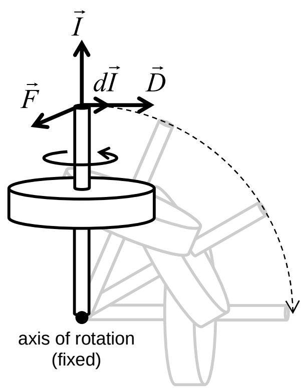

Figure 1.2. Example: change of the orientation of a rigid rotating body when the torque is acting upon it.

1.1.2. Classical magnetic dipole

Magnetic dipole is created by a flow of electric charge around a loop. Direction of the magnetic dipole is determined by the right hand grip rule, similar to the one shown in Figure 1.1 (four fingers point in the way of electric current, thumb shows the direction of magnetic dipole). *Magnetic dipole moment* is the measure of the strength of the magnetic dipole, equivalent to its ability to align with a given external magnetic field. Energy E of a magnetic dipole moment $\vec{\mu}$ in a magnetic field $\vec{B}$ is given by

$$E = -\vec{\mu} \cdot \vec{B} = -|\vec{\mu}||\vec{B}|\cos\theta = -\mu B \cos\theta\,. \tag{1.4}$$

In SI strength of a magnetic field is measured in Tesla (T), thus the unit of magnetic dipole moment is J/T. Magnetic dipole moment is aligned in magnetic field by a torque

$$\vec{D} = \vec{\mu} \times \vec{B}\,. \tag{1.5}$$

According to (1.3) torque leads to the change in the angular momentum:

$$\vec{\mu} \times \vec{B} = \frac{d\vec{I}}{dt} \tag{1.6}$$

and thus to the rotation of the magnetic dipole. Magnetic dipole which is not aligned with external magnetic field starts to oscillate around the energetically most stable orientation (see Figure 1.3) like a pendulum.

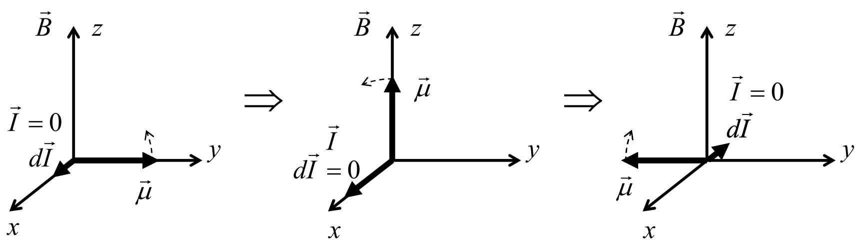

Figure 1.3. Oscillations of a magnetic dipole moment in magnetic field.

1.1.3. Classical magnetic dipole with angular momentum

Consider the body which has the magnetic dipole moment $\vec{\mu}$ and the classical intrinsic angular momentum $\vec{I}$ parallel to $\vec{\mu}$. We define

$$\vec{\mu} = \gamma \vec{I} \, . \tag{1.7}$$

Coefficient of proportionality, γ, is called *gyromagnetic ratio*. More precise term *magnetogyric ratio* is also sometimes used in the textbooks. Unit of γ is $T^{-1}s^{-1}$ (sometimes written as $rad \cdot T^{-1}s^{-1}$). From (1.6) and (1.7) it follows that the time evolution of magnetic dipole moment in magnetic field $\vec{B}$ is described by

$$\frac{d\vec{\mu}}{dt} = \gamma \vec{\mu} \times \vec{B} \, . \tag{1.8}$$

In order to demonstrate this motion we set the initial angle between $\vec{\mu}$ and $\vec{B}$ to 90°. Angular momenta at times t and $t + dt$ are illustrated in Figure 1.4.

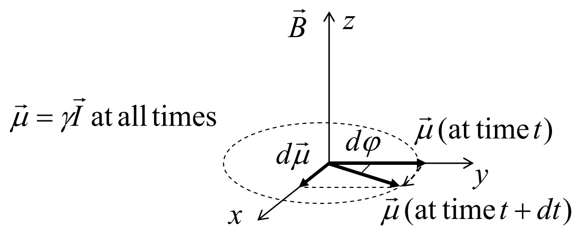

Figure 1.4. Precession of the magnetic moment in magnetic field in the presence of angular momentum.

At each moment of time the increment $d\vec{I}$ of the angular momentum is perpendicular to the magnetic moment $\vec{\mu}$ and thus to the angular momentum $\vec{I}$. Thus, at all times $\vec{I}$ and $\vec{\mu}$ remain in the *xy* plane. Then equation (1.6) can be rewritten as

$$\frac{dI}{dt} = \mu B = \gamma I B \, . \tag{1.9}$$

This motion is called *precession* of the magnetic dipole moment around the direction of external magnetic field $\vec{B}$. Let's find the angular velocity ω of the precession. By definition angular velocity is given by

$$\omega = \frac{d\varphi}{dt} \, . \tag{1.10}$$

From Figure 1.4 we obtain

$$dI = I \sin(-d\varphi) = -I d\varphi \, . \tag{1.11}$$

Note that angle increment $d\varphi$ was taken as negative as the positive angles in *xy* plane are counted anti-clockwise when observed from the positive end of *z* axis. Combining equations (1.9) and (1.11) we get

$$-\frac{Id\varphi}{dt} = \gamma IB \Rightarrow \frac{d\varphi}{dt} = -\gamma B \tag{1.12}$$

and thus

$$\omega = -\gamma B \,. \tag{1.13}$$

Angular velocity ω is called *Larmor frequency* of the precession.

1.2. Quantum-mechanical description of magnetic dipole

1.2.1. Nuclear spin

Spin is a basic non-classical property of some elementary particles. Spin is an abstract concept forced upon scientists by experimental evidence. It describes the angular momentum of a particle. Spin does not represent a rotation of a particle around its axis (as an Earth daily rotation) but is an intrinsic property, as are mass and charge. According to quantum mechanics the absolute value of angular momentum of a particle is

$$I = \sqrt{S(S+1)}\hbar \,, \tag{1.14}$$

where S is spin quantum number or simply spin. For some particles S is given by a whole integer, i.e. one of 0, 1, 2…. Such particles are called *bosons*. For other particles S is given by a half-integer, i.e. one of 1/2, 3/2, 5/2…. Such particles are called *fermions*. In Table 1 are listed few examples of atomic nuclei and their spins. Phrases like "proton has spin one-half" have to be understood in the sense of equation (1.14) with $S = 1/2$.

Table 1. Selected atomic nuclei and their spins.

Atomic nucleus	Spin quantum number S	Natural abundance, %
^{1}H	1/2	99.98
^{2}H	1	0.02
^{12}C	0	98.89
^{13}C	1/2	1.11
^{14}N	1	99.63
^{15}N	1/2	0.37
^{16}O	0	99.76
^{17}O	5/2	0.038

The projection of total angular momentum on the given direction, I_z, is quantized as well:

$$I_z = m\hbar \text{, where } m = -S, -S+1, ..., S-1, S \,. \tag{1.15}$$

Overall number of orientations is $2S+1$.

Consider the case of a nucleus with $S = 1/2$, such as ^{1}H, ^{19}F, ^{13}C, ^{15}N, ^{29}Si, ^{31}P etc. According to (1.15) such nucleus can have only two values of projection of angular momentum:

$$I_z = -\frac{1}{2}\hbar,\ \frac{1}{2}\hbar. \tag{1.16}$$

Following the standard nomenclature, we will often refer to these states (in Dirac notations) as

$$|\alpha\rangle \text{ (for } m = \frac{1}{2}\text{) and } |\beta\rangle \text{ (for } m = -\frac{1}{2}\text{).} \tag{1.17}$$

Projections of I on other axes (x and y) are not defined, as they can not be measured simultaneously with I_z. In quantum-mechanical terms, operators $\hat{I}_x$ and $\hat{I}_y$ do not commute with $\hat{I}_z$. This is illustrated in Figure 1.5, where undefined projections I_x and I_y are omitted. Note that in many books the undefined projections I_x and I_y are symbolised by conical shapes. This visualization has very limited applicability to more complex NMR phenomena and thus will be avoided in this course.

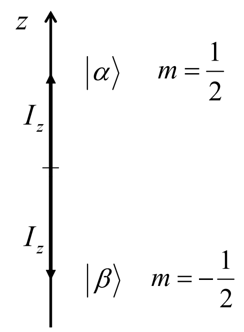

Figure 1.5. Orientation of angular momentum for a particle with spin 1/2 with respect to a given direction. Undefined I_x and I_y projections are omitted

In the absence of external fields the energies of states $|\alpha\rangle$ and $|\beta\rangle$ are equal. This degeneracy is removed in the presence of external magnetic field, as described below.

1.2.2. Nuclear magnetic moment

All nuclei with non-zero spin have also a magnetic dipole moment. In all cases magnetic dipole moment is parallel to the spin. The proportionality is given, according to (1.7), by the gyromagnetic ratio γ. Note, that γ can be either positive or negative. The values of gyromagnetic ratios are established experimentally. In Table 2 are given the values of γ for selected nuclei.

Table 2. Selected atomic nuclei and their gyromagnetic ratios.

Atomic nucleus	Gyromagnetic ratio γ $/10^6 \cdot \mathrm{rad \cdot T^{-1} s^{-1}}$
^{1}H	267.5
^{2}H	41.1
^{12}C	-
^{13}C	67.3
^{14}N	19.3
^{15}N	-27.1
^{16}O	-
^{17}O	-36.3

Consider the magnetic field being parallel to the *z*-axis. As spin can have only certain orientations with respect to given direction (*z*-axis in this case), so does the magnetic dipole moment. Combining equations (1.15) and (1.7) we get for the projection of the magnetic dipole moment

$$\mu_z = m\gamma\hbar . \tag{1.18}$$

According to (1.4), magnetic dipole moment μ has energy

$$E_m = -m\gamma\hbar B . \tag{1.19}$$

For a spin ½ with positive gyromagnetic ratio γ we get two energy levels

$$\begin{aligned} E_{\frac{1}{2}} &= -\frac{1}{2}\gamma\hbar B \ \ (\text{state } |\alpha\rangle \text{) and} \\ E_{-\frac{1}{2}} &= \frac{1}{2}\gamma\hbar B \ \ (\text{state } |\beta\rangle \text{)} \end{aligned} \tag{1.20}$$

split by

$$\Delta E = E_{-\frac{1}{2}} - E_{\frac{1}{2}} = \frac{1}{2}\gamma\hbar B - \left(-\frac{1}{2}\gamma\hbar B\right) = \gamma\hbar B = \hbar\omega = h\nu . \tag{1.21}$$

Splitting of the energy levels in the magnetic field is called *Zeeman splitting*. Energy level diagram for single spin 1/2 is given in Figure 1.6.

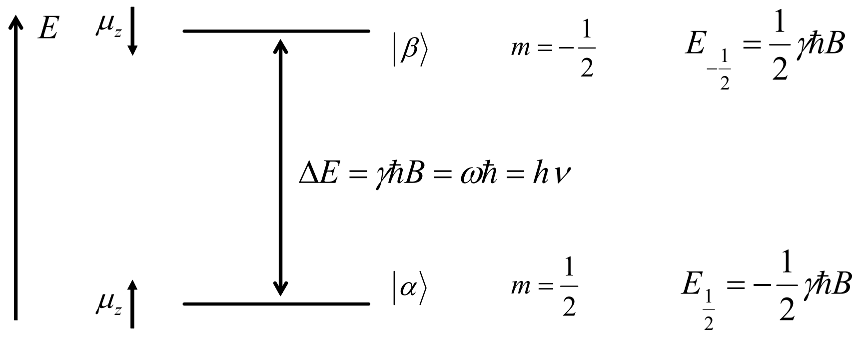

Figure 1.6. Energy level diagram for a single spin 1/2 in magnetic field.

Equation (1.21) links the classical description of the "magnetic dipole with parallel angular momentum" with the quantum-mechanical "nuclear spin". Using classical physics we found out that magnetic moment precesses around the magnetic field with frequency ω. In quantum mechanics this frequency corresponds to transition between two stationary energy states.

1.2.3. Ensemble of nuclear spins 1/2 in magnetic field

Consider an ensemble of nuclear spins 1/2. In the absence of magnetic field $|\alpha\rangle$ and $|\beta\rangle$ states are equally populated (Figure 1.7a). In the presence of magnetic field the population of energy levels change and finally reaches the thermal equilibrium (Figure 1.7b). The stronger is the magnetic field $\vec{B}$ the bigger is the difference in the population of energy levels.

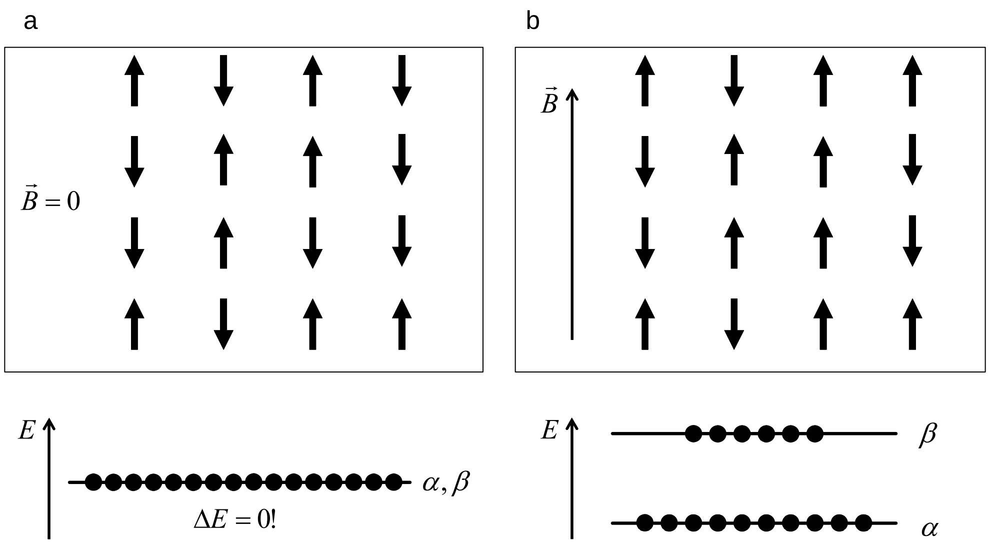

Figure 1.7. Ensemble of nuclear spins ½ in the absence (a) and presence (b) of magnetic field.

Boltzmann distribution in thermal equilibrium gives

$$\frac{N_\beta}{N_\alpha}=exp\left(-\frac{\Delta E}{kT}\right)\approx 1-\frac{\Delta E}{kT}, \tag{1.22}$$

where the energy difference is given by (1.21). If we define population fractions as

$$x_\alpha = \frac{N_\alpha}{N_\alpha + N_\beta},\ x_\beta = \frac{N_\beta}{N_\alpha + N_\beta},\ x_\alpha + x_\beta = 1 \tag{1.23}$$

then we obtain

$$x_\alpha = \frac{1}{1+\frac{N_\beta}{N_\alpha}} \approx \frac{1}{1+1+\frac{\Delta E}{kT}} = \frac{1}{2+\frac{\Delta E}{kT}},\ x_\beta = \frac{1}{1+\frac{N_\alpha}{N_\beta}} \approx \frac{1}{1+1-\frac{\Delta E}{kT}} = \frac{1}{2-\frac{\Delta E}{kT}}. \tag{1.24}$$

For example, the energy levels splitting for ^{1}H in magnetic field $B = 10T$ at $T = 298K$ is

$$\frac{\Delta E}{kT} = \frac{\gamma\hbar B}{kT} = \frac{267.5\cdot 10^6 rad\cdot T^{-1}s^{-1}\cdot 1.05\cdot 10^{-34} Js\cdot rad^{-1}\cdot 10T}{1.38\cdot 10^{-23} JK^{-1}\cdot 298K} = 0.000068 \tag{1.25}$$

and thus the population fractions are

$$x_\alpha = 0.499983 \text{ and } x_\beta = 0.500017 \tag{1.26}$$

1.3. Classical description of NMR experiment

1.3.1. Macroscopic magnetisation

The sum of individual magnetic moments of nuclei is *macroscopic magnetisation* (or "*polarization*" or "*net magnetisation*"):

$$\vec{M}_\infty = \sum_i \vec{\mu}_{zi} = \begin{pmatrix} 0 \\ 0 \\ M_\infty \end{pmatrix}. \tag{1.27}$$

Here, index i numbers all the nuclear spins in the system and $\vec{\mu}_{zi}$ stands for projection of the magnetic dipole moment of spin i on the direction of external magnetic field. The subscript ∞ denotes the magnetisation in the thermodynamic equilibrium.

It can be anticipated from (1.21)-(1.23) that

$$\begin{aligned} &M_\infty = 0 \text{ for } \vec{B} = 0 \text{ and} \\ &M_\infty = const\cdot\left(x_\alpha - x_\beta\right) \text{ for } \vec{B} \neq 0. \end{aligned} \tag{1.28}$$

1.3.2. Overview of the NMR experiment

In brief, the typical NMR experiment can be pictured as follows. The NMR sample is placed inside the magnet, which produces the external magnetic field $\vec{B}_0$ (See Figure 1.8a) and the macroscopic magnetisation $\vec{M}$ is built parallel to $\vec{B}_0$. Then the radio-frequency transmitter produces the magnetic field $\vec{B}_1$, oscillating with frequency ω_{ref} along the axis, perpendicular to $\vec{B}_0$. Magnetic field $\vec{B}_1$ is called "*the pulse*". The interaction of the magnetisation $\vec{M}$ with the overall magnetic field $\vec{B}_0 + \vec{B}_1$ will be considered in detail in the following sections. For now, we take for granted that by the end of the pulse the magnetisation $\vec{M}$ is oriented perpendicular to $\vec{B}_0$ (Figure 1.8b). Then the oscillating magnetic field $\vec{B}_1$ is switched off. In the absence of $\vec{B}_1$ the magnetisation $\vec{M}$ starts to precess around $\vec{B}_0$ with the frequency $\omega_0 = \gamma B_0$. This precession creates the alternating voltage in the NMR coil. The alternating voltage is recorded and called *Free Induction Decay* (*FID*). With time, the magnetisation relaxes back to the equilibrium and the FID signal decays. The spectrum of the sample is the Fourier Transformation (FT) of the FID.

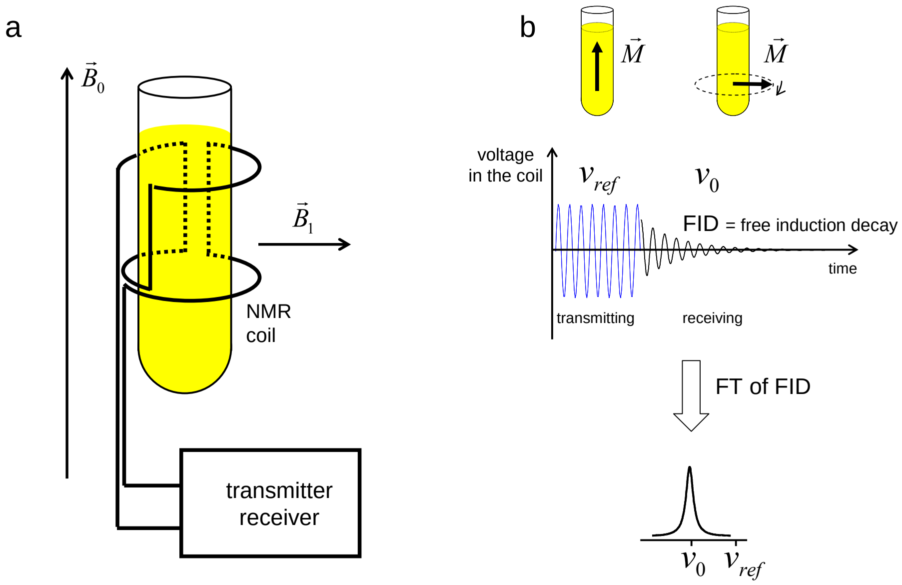

Figure 1.8. Overview of the NMR experiment. (a) position of the sample in the external magnetic field $\vec{B}_0$ and orientation of the magnetic field of the pulse, $\vec{B}_1$. (b) Voltage in the NMR coil as a function of time; spectrum is recorded as a Fourier transformation of the FID signal.

The necessity of the experimental setup described above will be justified in the following sections.

1.3.3. Laboratory and rotating frames

Description of the NMR experiments simplifies by introducing two systems of coordinates:

a) "laboratory" frame with coordinate axes x, y, z.

b) "rotating" frame with coordinate axes u, υ, z, which rotates around the z-axis of laboratory frame with the angular velocity ω_{ref} as depicted in Figure 1.9.

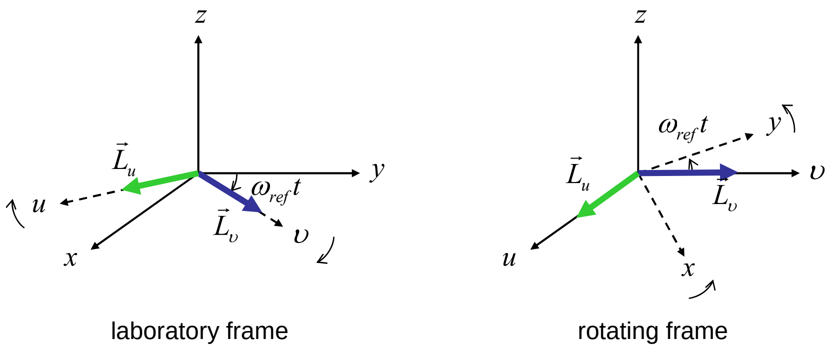

Figure 1.9. Laboratory and rotating frames.

Consider vectors $\vec{L}_u$ and $\vec{L}_\upsilon$, which are parallel to the u and υ axes of the rotating frame (see Figure 1.9). The projections of $\vec{L}_u$ and $\vec{L}_\upsilon$ on the x and y axes of the laboratory frame are given by

$$\begin{aligned}
&\text{component of } \vec{L}_u \text{ along the } x\text{-axis } L_u^x = L_u \cos\omega_{ref} t\,,\\
&\text{component of } \vec{L}_u \text{ along the } y\text{-axis } L_u^y = -L_u \sin\omega_{ref} t\,,\\
&\text{component of } \vec{L}_\upsilon \text{ along the } x\text{-axis } L_\upsilon^x = L_\upsilon \sin\omega_{ref} t\,,\\
&\text{component of } \vec{L}_\upsilon \text{ along the } y\text{-axis } L_\upsilon^y = L_\upsilon \cos\omega_{ref} t\,.
\end{aligned} \tag{1.29}$$

For the total projections we get (in the matrix form):

$$\begin{pmatrix} L_x \\ L_y \\ L_z \end{pmatrix} = \begin{pmatrix} L_u^x + L_\upsilon^x \\ L_u^y + L_\upsilon^y \\ L_z \end{pmatrix} = \begin{pmatrix} L_u \cos\omega_{ref} t + L_\upsilon \sin\omega_{ref} t \\ -L_u \sin\omega_{ref} t + L_\upsilon \cos\omega_{ref} t \\ L_z \end{pmatrix} \tag{1.30}$$

Equation (1.30) can be solved to find the reverse transformation:

$$\begin{pmatrix} L_u \\ L_\upsilon \\ L_z \end{pmatrix} = \begin{pmatrix} L_x \cos\omega_{ref} t - L_y \sin\omega_{ref} t \\ L_x \sin\omega_{ref} t + L_y \cos\omega_{ref} t \\ L_z \end{pmatrix} \tag{1.31}$$

For the time derivatives of vector $\vec{L}$ we get in rotating frame:

$$\begin{aligned}
\frac{dL_u}{dt} &= \frac{dL_x}{dt}\cos\omega_{ref} t - \frac{dL_y}{dt}\sin\omega_{ref} t - \omega_{ref} L_\upsilon\,,\\
\frac{dL_\upsilon}{dt} &= \frac{dL_x}{dt}\sin\omega_{ref} t + \frac{dL_y}{dt}\cos\omega_{ref} t + \omega_{ref} L_u\,,\\
\frac{dL_z}{dt} &= \frac{dL_z}{dt}\,.
\end{aligned} \tag{1.32}$$

1.3.4. Magnetic field of the pulse

The magnetic field of the pulse along the x-axis is given by

$$\vec{B}_1 = \begin{pmatrix} 2B_1 \cos\omega_{ref} t \\ 0 \\ 0 \end{pmatrix}, \qquad (1.33)$$

where the factor 2 is introduced for convenience.

We can represent $\vec{B}_1$ as the sum of two magnetic fields:

$$\vec{B}_1 = \vec{B}_1^{z} + \vec{B}_1^{-z}, \qquad (1.34)$$

where

$$\vec{B}_1^{z} = \begin{pmatrix} B_1 \cos\omega_{ref} t \\ B_1 \sin\omega_{ref} t \\ 0 \end{pmatrix} \text{ and } \vec{B}_1^{-z} = \begin{pmatrix} B_1 \cos\omega_{ref} t \\ -B_1 \sin\omega_{ref} t \\ 0 \end{pmatrix}. \qquad (1.35)$$

Magnetic fields $\vec{B}_1^{z}$ and $\vec{B}_1^{-z}$ describe the magnetic fields rotating in opposite direction around the z-axis in the laboratory frame. This is illustrated in Figure 1.10, where the transmitter/receiver coil is schematically shown as well.

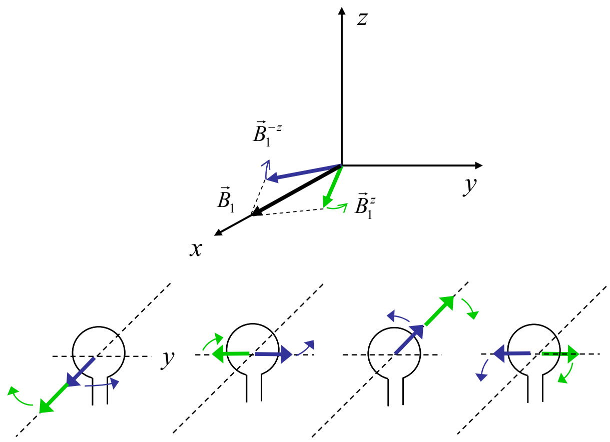

Figure 1.10. Linear polarized magnetic field of the pulse $\vec{B}_1$ represented as a sum of two circular polarized magnetic fields, $\vec{B}_1^{z}$ and $\vec{B}_1^{-z}$. Transmitter/receiver coil is depicted with the solid black line.

According to (1.31), the magnetic fields $\vec{B}_1^{z}$ and $\vec{B}_1^{-z}$ in the rotating frame are given by

$$\vec{B}_1^{-z}(in\, rotating\ frame) = \begin{pmatrix} B_1 \cos\omega_{ref} t \cos\omega_{ref} t + B_1 \sin\omega_{ref} t \sin\omega_{ref} t \\ B_1 \cos\omega_{ref} t \sin\omega_{ref} t - B_1 \sin\omega_{ref} t \cos\omega_{ref} t \\ 0 \end{pmatrix} = \begin{pmatrix} B_1 \\ 0 \\ 0 \end{pmatrix}, \qquad (1.36)$$

$$\vec{B}_1^z(in\,rotating\;frame)=\begin{pmatrix} B_1\cos\omega_{ref}t\cos\omega_{ref}t-B_1\sin\omega_{ref}t\sin\omega_{ref}t \\ B_1\cos\omega_{ref}t\sin\omega_{ref}t+B_1\sin\omega_{ref}t\cos\omega_{ref}t \\ 0 \end{pmatrix}=\begin{pmatrix} B_1\cos 2\omega_{ref}t \\ B_1\sin 2\omega_{ref}t \\ 0 \end{pmatrix}.$$

It can be shown that the "fast rotating" magnetic field $\vec{B}_1^z(in\,rotating\;frame)$ does not influence the time evolution of magnetisation $\vec{M}$. Thus, we neglect it and later will consider only $\vec{B}_1^{-z}$ as the magnetic field of the pulse. See also Figure 1.11.

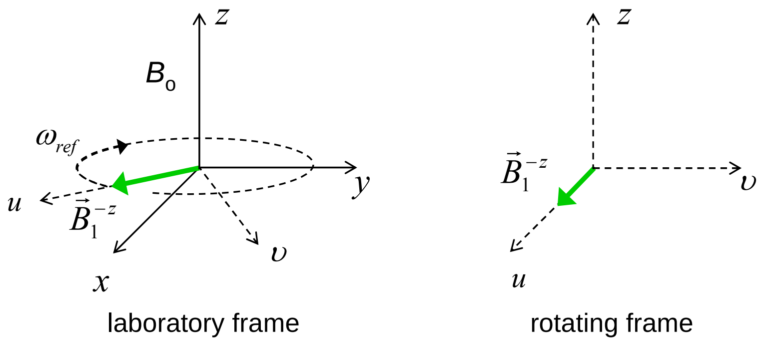

Figure 1.11. Magnetic field $\vec{B}_1^{-z}$ in laboratory frame and in rotating frame.

1.3.5. Bloch equations

Equation (1.8) can be re-written for the individual components of the net magnetisation as

$$\begin{aligned} \frac{dM_x}{dt} &= \gamma(M_yB_z - M_zB_y), \\ \frac{dM_y}{dt} &= \gamma(-M_xB_z + M_zB_x),\,. \\ \frac{dM_z}{dt} &= \gamma(M_xB_y - M_yB_x) \end{aligned} \tag{1.37}$$

These equations describe the infinite precession. In reality, however, the system which is not in thermodynamic equilibrium will gradually come to it. Thus, from every starting conditions magnetisation $\vec{M}$ will eventually reach its equilibrium value (1.27). It can be anticipated that the rate with which magnetisation $\vec{M}$ changes is proportional to how far it is from its equilibrium value $\vec{M}_\infty$. Thus, to account for this *relaxation* of the magnetisation we introduce additional terms in (1.37):

$$\frac{dM_x}{dt} = \gamma\left(M_y B_z - M_z B_y\right) - \frac{M_x}{T_2},$$
$$\frac{dM_y}{dt} = \gamma\left(-M_x B_z + M_z B_x\right) - \frac{M_y}{T_2}, \tag{1.38}$$
$$\frac{dM_z}{dt} = \gamma\left(M_x B_y - M_y B_x\right) - \frac{M_z - M_\infty}{T_1}$$

Equations (1.38) were first formulated by Bloch in 1946 and were later confirmed by the quantum statistics.

The *z*-component of magnetisation is built by the spin flips involving the energy transfer between spin system and the environment ("lattice"), which requires the magnetic field oscillations with the Larmor frequency. This process is called "*spin-lattice relaxation*" or "*longitudinal relaxation*". The corresponding characteristic time T_1 is called longitudinal or spin-lattice *relaxation time*.

The characteristic time T_2 with which the *x*- and *y*-components of magnetisation are relaxing to their equilibrium values can be different from T_1. Indeed, each spin experiences the external B_0 along with the local additional fields, generated by the neighbouring spins. As a result, the spins will precess with different frequency, depending on the actual field. Some spins will be "ahead" and some will be "behind" the ideal Larmor precession, leading to the "*defocusing*" in the net magnetisation. This process is called *transverse relaxation* and T_2 is called *transverse relaxation time*.

Relaxation processes are illustrated in Figure 1.12.

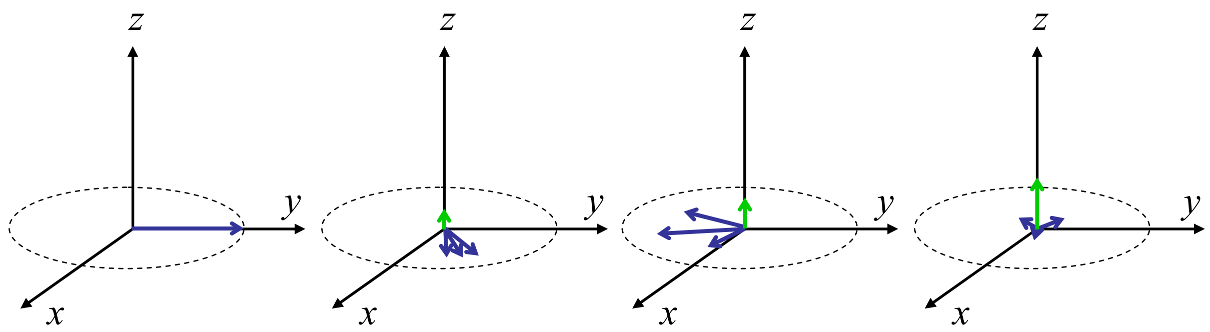

Figure 1.12. Defocusing of the net magnetisation in the *xy* plane of the laboratory frame (T_2 relaxation) and building up of the magnetization in along *z* axis (T_1 relaxation).

Combining (1.38) and (1.32), for the time derivative on magnetisation components in the rotating frame we get:

$$\begin{aligned}
\frac{dM_u}{dt} &= \left(\gamma\left(M_y B_z - M_z B_y\right) - \frac{M_x}{T_2}\right)\cos\omega_{ref}t - \left(\gamma\left(-M_x B_z + M_z B_x\right) - \frac{M_y}{T_2}\right)\sin\omega_{ref}t - \omega_{ref}M_\upsilon \\
\frac{dM_\upsilon}{dt} &= \left(\gamma\left(M_y B_z - M_z B_y\right) - \frac{M_x}{T_2}\right)\sin\omega_{ref}t + \left(\gamma\left(-M_x B_z + M_z B_x\right) - \frac{M_y}{T_2}\right)\cos\omega_{ref}t + \omega_{ref}M_u \\
\frac{dM_z}{dt} &= \gamma\left(M_x B_y - M_y B_x\right) - \frac{M_z - M_\infty}{T_1}
\end{aligned} \tag{1.39}$$

Using (1.31) we simplify:

$$\begin{aligned}
\frac{dM_u}{dt} &= \gamma\left(M_y B_z - M_z B_y\right)\cos\omega_{ref}t - \gamma\left(-M_x B_z + M_z B_x\right)\sin\omega_{ref}t - \frac{M_u}{T_2} - \omega_{ref}M_\upsilon \\
\frac{dM_\upsilon}{dt} &= \gamma\left(M_y B_z - M_z B_y\right)\sin\omega_{ref}t + \gamma\left(-M_x B_z + M_z B_x\right)\cos\omega_{ref}t - \frac{M_\upsilon}{T_2} + \omega_{ref}M_u \\
\frac{dM_z}{dt} &= \gamma\left(M_x B_y - M_y B_x\right) - \frac{M_z - M_\infty}{T_1}
\end{aligned} \tag{1.40}$$

The magnetic field $\vec{B}$ consists of the external field $\vec{B}_0$ and the magnetic field of the pulse $\vec{B}_1^{-z}$:

$$\vec{B} = \vec{B}_0 + \vec{B}_1^{-z} = \begin{pmatrix} 0 \\ 0 \\ B_0 \end{pmatrix} + \begin{pmatrix} B_1\cos\omega_{ref}t \\ -B_1\sin\omega_{ref}t \\ 0 \end{pmatrix} = \begin{pmatrix} B_1\cos\omega_{ref}t \\ -B_1\sin\omega_{ref}t \\ B_0 \end{pmatrix}. \tag{1.41}$$

If we define

$$\begin{aligned}
\omega_0 &= \gamma B_0, \\
\omega_1 &= \gamma B_1
\end{aligned} \tag{1.42}$$

we can re-write (1.40) as

$$\begin{aligned}
\frac{dM_u}{dt} &= \left(M_y\omega_0 + M_z\omega_1\sin\omega_{ref}t\right)\cos\omega_{ref}t - \left(-M_x\omega_0 + M_z\omega_1\cos\omega_{ref}t\right)\sin\omega_{ref}t - \frac{M_u}{T_2} - \omega_{ref}M_\upsilon \\
\frac{dM_\upsilon}{dt} &= \left(M_y\omega_0 + M_z\omega_1\sin\omega_{ref}t\right)\sin\omega_{ref}t + \left(-M_x\omega_0 + M_z\omega_1\cos\omega_{ref}t\right)\cos\omega_{ref}t - \frac{M_\upsilon}{T_2} + \omega_{ref}M_u \\
\frac{dM_z}{dt} &= \left(-M_x\omega_1\sin\omega_{ref}t - M_y\omega_1\cos\omega_{ref}t\right) - \frac{M_z - M_\infty}{T_1}
\end{aligned} \tag{1.43}$$

Further simplifications give:

$$\frac{dM_u}{dt} = (\omega_0 - \omega_{ref})M_\upsilon - \frac{M_u}{T_2}$$
$$\frac{dM_\upsilon}{dt} = -(\omega_0 - \omega_{ref})M_u + \omega_1 M_z - \frac{M_\upsilon}{T_2} \qquad (1.44)$$
$$\frac{dM_z}{dt} = -M_\upsilon \omega_1 - \frac{M_z - M_\infty}{T_1}$$

Equations (1.44) are known as Bloch equations in rotating frame. Once again, here ω_0 is the resonance frequency of the observed nucleus, ω_{ref} is the frequency of the pulse and ω_1 is the precession frequency of the magnetisation in the rotating frame during the pulse ("pulse intensity").

1.3.6. Pulse!

In this section we will discuss the time evolution of $\vec{M}$ during the pulse, i.e. when magnetic field $\vec{B}_1 \neq 0$. For better understanding of the physical sense, we also assume that

$$\omega_{ref} \approx \omega_0,$$
$$T_1 >> 1, \qquad (1.45)$$
$$T_2 >> 1$$

In this case (1.44) is simplified to

$$\frac{dM_u}{dt} = 0$$
$$\frac{dM_\upsilon}{dt} = \omega_1 M_z \qquad (1.46)$$
$$\frac{dM_z}{dt} = -M_\upsilon \omega_1$$

As it can be checked by derivation, solution of equations (1.46) is as follows:

$$M_u = 0$$
$$M_\upsilon = M_\infty \sin \omega_1 t \qquad (1.47)$$
$$M_z = M_\infty \cos \omega_1 t$$

Equations (1.47) describe the rotation of magnetisation around u axis of the rotating frame with the angular velocity ω_1. This motion is illustrated in Figure 1.13b. Figure 1.13a illustrates the same motion is the laboratory frame.

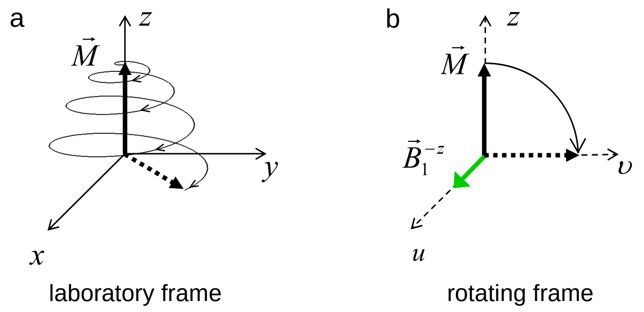

Figure 1.13. Time evolution of $\vec{M}$ during the pulse, as seen in the rotating frame.

The duration of the pulse needed to put the magnetisation $\vec{M}$ into the *xy*-plane (or $u\upsilon$-plane of the rotating frame) is called the duration of the "*90-degree pulse*". From (1.47) it follows that:

$$\omega_1 t_{90^\circ} = \frac{\pi}{2} \Rightarrow t_{90^\circ} = \frac{\pi}{2\omega_1} = \frac{\pi}{2\gamma B_1} \tag{1.48}$$

1.3.7. Free induction decay

In this section we will discuss the time evolution of $\vec{M}$ after the 90-degree pulse, i.e. when $\vec{B}_1 = 0$. According to (1.47) and (1.48), the initial conditions are

$$\vec{M}(in\ rotating\ frame) = \begin{pmatrix} 0 \\ M_\infty \\ 0 \end{pmatrix}. \tag{1.49}$$

We assume that

$$T_1 >> 1, \tag{1.50}$$

though T_2 can be short. In this case the Bloch equation can be re-written as

$$\begin{aligned} \frac{dM_u}{dt} &= (\omega_0 - \omega_{ref})M_\upsilon - \frac{M_u}{T_2} \\ \frac{dM_\upsilon}{dt} &= -(\omega_0 - \omega_{ref})M_u - \frac{M_\upsilon}{T_2} \\ \frac{dM_z}{dt} &= 0 \end{aligned} \tag{1.51}$$

As it can be checked by derivation, solution of equations (1.51) is as follows:

$$
\begin{aligned}
M_u &= M_\infty e^{-t/T_2} \sin(\omega_0 - \omega_{ref})t \\
M_\upsilon &= M_\infty e^{-t/T_2} \cos(\omega_0 - \omega_{ref})t \\
M_z &= 0
\end{aligned}
\tag{1.52}
$$

This time evolution is illustrated in Figure 1.14

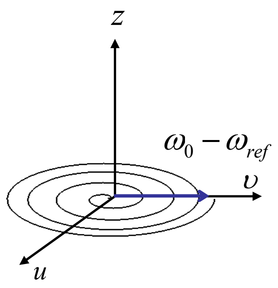

Figure 1.14. Time evolution of $\vec{M}$ in *xy*-plane after the pulse (FID, Free Indiction decay). Note the angular velocity of the motion.

Using transformation (1.30) it can be shown that in the laboratory frame we obtain from (1.52):

$$
\begin{aligned}
M_x &= M_\infty e^{-t/T_2} \sin \omega_0 t \\
M_y &= M_\infty e^{-t/T_2} \cos \omega_0 t \\
M_z &= 0
\end{aligned}
\tag{1.53}
$$

The time dependence of the voltage in the transmitter/receiver coil is depicted in Figure 1.15.

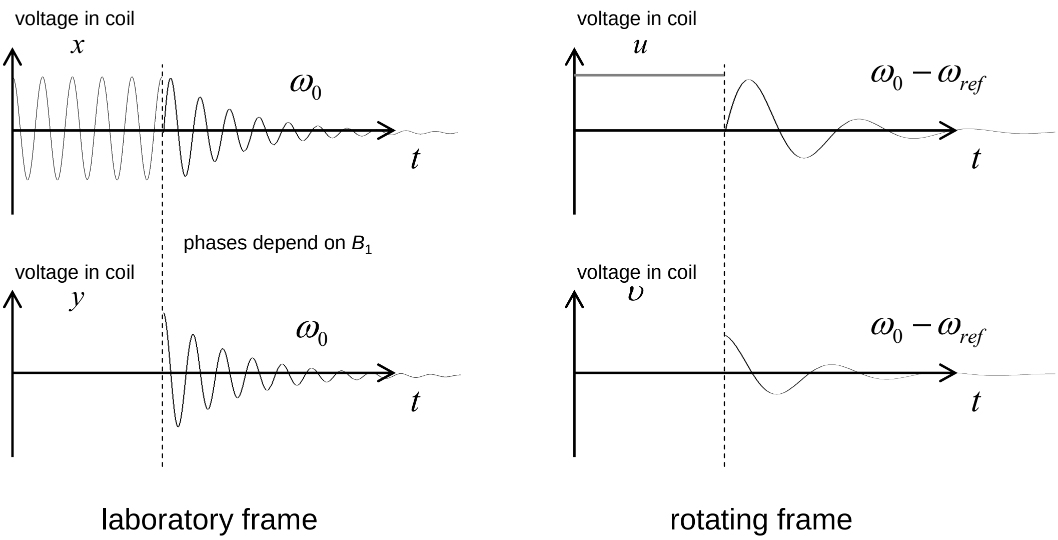

Figure 1.15. Time evolution of the voltage in the transmitter/receiver coil during the NMR experiment.

1.3.8. Fourier Transformation of FID. Spectral lines

Fourier transformation of any time-dependent function $f(t)$ is defined as

$$f(\omega)=\frac{1}{\sqrt{2\pi}}\int_{-\infty}^{+\infty} f(t)e^{-i\omega t}\,dt \tag{1.54}$$

Thus, the Fourier transformation of (1.53) is

$$\begin{aligned} M_x(\omega) &= \frac{1}{\sqrt{2\pi}}\int_{0}^{+\infty} M_\infty e^{-t/T_2}\sin\omega_0 t\cdot e^{-i\omega t}\,dt \\ M_y(\omega) &= \frac{1}{\sqrt{2\pi}}\int_{-\infty}^{+\infty} M_\infty e^{-t/T_2}\cos\omega_0 t\cdot e^{-i\omega t}\,dt \end{aligned} \tag{1.55}$$

Using the following expressions:

$$\begin{aligned} \sin x &= \frac{e^{ix}-e^{-ix}}{2i} \\ \cos x &= \frac{e^{ix}+e^{-ix}}{2} \end{aligned} \tag{1.56}$$

we obtain:

$$\begin{aligned} M_x(\omega) &= \frac{M_\infty}{2i\sqrt{2\pi}}\int_{0}^{+\infty} e^{-t/T_2}\left(e^{i\omega_o t}-e^{-i\omega_o t}\right)\cdot e^{-i\omega t}\,dt \\ M_y(\omega) &= \frac{M_\infty}{2\sqrt{2\pi}}\int_{0}^{+\infty} e^{-t/T_2}\left(e^{i\omega_o t}+e^{-i\omega_o t}\right)\cdot e^{-i\omega t}\,dt \end{aligned} \tag{1.57}$$

Below we do the integration for the $M_x(\omega)$. For the $M_y(\omega)$ the math is very similar. Integration gives:

$$M_x(\omega) = -\frac{M_\infty}{2i\sqrt{2\pi}}\left(\frac{1}{\frac{1}{T_2}-i(\omega_o-\omega)}\right)e^{-\left(\frac{1}{T_2}-i(\omega_o-\omega)\right)t}\Bigg|_0^{+\infty} + \frac{M_\infty}{2i\sqrt{2\pi}}\left(\frac{1}{\frac{1}{T_2}+i(\omega_o+\omega)}\right)e^{-\left(\frac{1}{T_2}+i(\omega_o+\omega)\right)t}\Bigg|_0^{+\infty} \tag{1.58}$$

Using the limits of integration we get

$$M_x(\omega) = \frac{M_\infty}{2i\sqrt{2\pi}}\left(\frac{1}{\frac{1}{T_2}-i(\omega_o-\omega)}\right) - \frac{M_\infty}{2i\sqrt{2\pi}}\left(\frac{1}{\frac{1}{T_2}+i(\omega_o+\omega)}\right). \tag{1.59}$$

After some re-ordering it gives:

$$M_x(\omega) = -iL(\omega_o - \omega) + D(\omega_o - \omega) + iL(\omega_o + \omega) + D(\omega_o + \omega). \tag{1.60}$$

and

$$M_y(\omega) = L(\omega_o - \omega) + iD(\omega_o - \omega) + L(\omega_o + \omega) - iD(\omega_o + \omega) \tag{1.61}$$

where

$$L(\omega_o \pm \omega) = \frac{M_\infty}{2\sqrt{2\pi}} \frac{\frac{1}{T_2}}{\left(\frac{1}{T_2}\right)^2 + (\omega_o \pm \omega)^2} \text{ and } D(\omega_o \pm \omega) = \frac{M_\infty}{2\sqrt{2\pi}} \frac{\omega_o \pm \omega}{\left(\frac{1}{T_2}\right)^2 + (\omega_o \pm \omega)^2}. \tag{1.62}$$

The shapes of the $L(\omega_o - \omega)$ and $D(\omega_o - \omega)$ functions are shown in Figure 1.16.

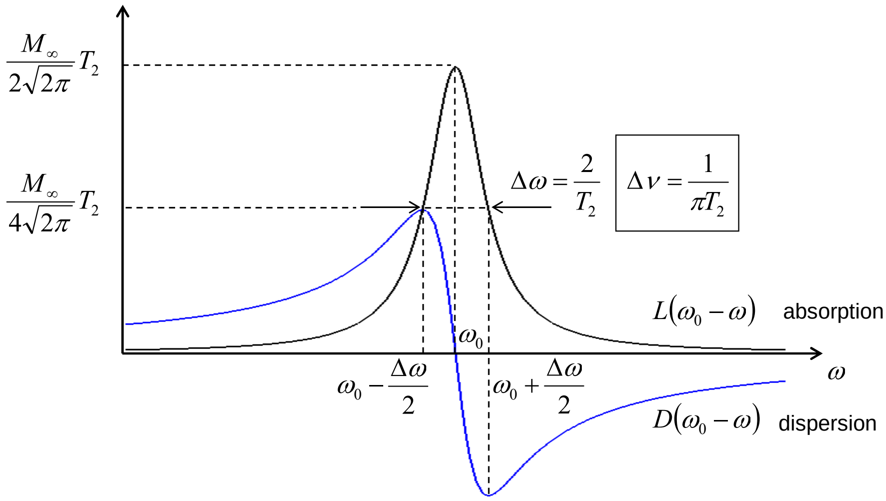

Figure 1.16. Lineshapes of the Lorentz and dispersion curves.

From (1.62) it follows that the intensity of $L(\omega_o - \omega)$ at maximum if given by $\frac{M_\infty}{2\sqrt{2\pi}}T_2$ and the width of the spectral line at half-height is given by

$$\Delta\omega = \frac{2}{T_2} \text{ or } \Delta\nu = \frac{1}{\pi T_2}. \tag{1.63}$$

In other words, the faster the magnetisation decays (shorter T_2 time), the broader is the spectral line (bigger $\Delta\nu$).

In also follows from (1.62) that

$$\int_{-\infty}^{+\infty} L(\omega_o - \omega) d\omega = \frac{1}{2}\sqrt{\frac{\pi}{2}} M_\infty. \tag{1.64}$$

The physical meaning of (1.64) is as follows. The integrated intensity of the spectral line is proportional to the equilibrium magnetization M_∞, which is, in turn, proportional to the population difference between spin energy levels. Thus, the integrated intensity of the line is proportional to the number of nuclei, contributing to the line.

In modern spectrometers the free induction decay is measured by two detectors, oriented by the 90-degree angle. By quadrature detection one registers (after Fourier transform)

$$M_y(\omega)+iM_x(\omega)=2L(\omega_o-\omega)+2iD(\omega_o-\omega). \tag{1.65}$$

The absorption spectrum is the real part and the dispersion spectrum is the imaginary part of (1.71):

$$\begin{aligned}\mathrm{Re}\left(M_y(\omega)+iM_x(\omega)\right)&=2L(\omega_o-\omega)\\ \mathrm{Im}\left(M_y(\omega)+iM_x(\omega)\right)&=2D(\omega_o-\omega).\end{aligned} \tag{1.66}$$

2. Chemical shielding

2.1. Origins of chemical shielding

On the electric charge q moving with velocity $\vec{V}$ in the magnetic field $\vec{B}_0$ acts the Lorentz force

$$\vec{F}=q\vec{V}\times\vec{B}_0. \tag{2.1}$$

Equation (2.1) describes the rotation of the charge around the direction of the magnetic field. The motion of the electron under the influence of the Lorentz force is shown in Figure 2.1

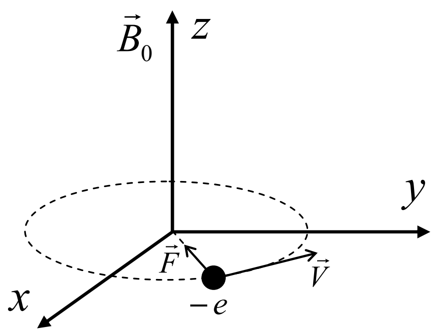

Figure 2.1. Lorentz force acting on the electron.

Circulating electron creates the electric current. The electric current, in turn, creates the magnetic field $\vec{B}_{induced}$. In the place of the nucleus $\vec{B}_{induced}$ is directed opposite (anti-parallel) to the external magnetic field $\vec{B}_0$, as illustrated in Figure 2.2.

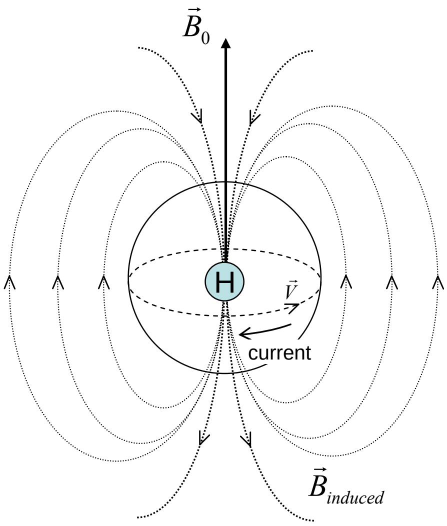

Figure 2.2. Magnetic field induced by electron moving around the nucleus in the magnetic field $\vec{B}_0$.

In short, the external magnetic field induces currents in the electron could, which decrease the magnetic field, experienced by the nucleus. This effect is called "*shielding*" of "*screening*" of the nucleus.

2.2. Chemical shift

The effective magnetic field, experienced by the nucleus, is given by

$$\vec{B} = \vec{B}_0 + \vec{B}_{induced} . \tag{2.2}$$

By looking at (2.1) one can anticipate that the induced field $\vec{B}_{induced}$ is not only anti-parallel, but also directly proportional to the external field $\vec{B}_0$. Thus, we re-write (2.2) as

$$\vec{B} = (1-\sigma)\vec{B}_0 , \tag{2.3}$$

where the positive coefficient σ is field-independent and is called *shielding constant*. The resonance frequency of the nucleus is then given by

$$\nu = \frac{\omega}{2\pi} = \frac{\gamma B}{2\pi} = \frac{\gamma B_0 (1-\sigma)}{2\pi} . \tag{2.4}$$

As different spectrometers have different magnetic fields, it is convenient to define the field-independent *chemical shift* as

$$\delta = \frac{\nu - \nu_{st}}{\nu_{st}} \cdot 10^6, \tag{2.5}$$

where ν_{st} is the resonance frequency of the selected standard and factor 10^6 is introduced for convenience. Using (2.4) we obtain:

$$\delta = \frac{\frac{\gamma}{2\pi} B_0 (1 - \sigma - 1 + \sigma_{st})}{\frac{\gamma}{2\pi} B_0 (1 - \sigma_{st})} \cdot 10^6 = \frac{\sigma_{st} - \sigma}{1 - \sigma_{st}} \cdot 10^6. \tag{2.6}$$

Because of the scaling factor 10^6 the "units" for the chemical shift are *parts per million* or simply *ppm*. The chemical shift of standard is, obviously, 0 ppm. Different molecules are selected as standards for different nuclei. Below are given the most often used ones:

for ^{1}H: $(CH_3)_4Si$

for ^{13}C: $(CH_3)_4Si$

for ^{15}N: NH_4Cl, NO_2CH_3, Glycine

It is generally accepted that the chemical shifts are shown growing from right to left. Nuclei showing higher values of the chemical shift are called "*less shielded*" ("*deshielded*"), while those with lower chemical shift are "*more shielded*". The region of higher chemical shifts is called "*low field*" and the region with lower chemical shifts is called "*high field*".

This terminology was created in 50's when NMR spectra were recorded using the magnetic field sweep instead of modern radio-frequency pulses. Thus, in order to come into resonance with the fixed frequency less shielded nuclei needed less strong magnetic field.

Chemical shift axis is shown in Figure 2.3a. Figure 2.3b shows the typical ^{1}H chemical shifts for some functional groups.

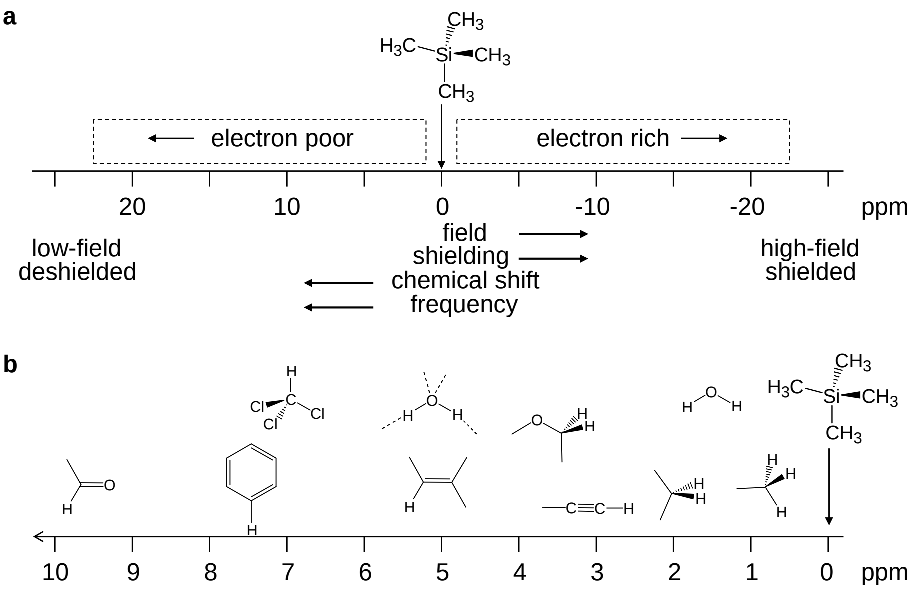

Figure 2.3. (a) Chemical shift axis. (b) Typical ^{1}H chemical shifts for some functional groups.

The nuclear shielding depends on the molecular orientation. Consider, for example, the ^{1}H chemical shift of the proton in the FH molecule. When the molecular axis is perpendicular to the external magnetic field (Figure 2.4a), the magnetic field created by the electron shell of fluorine at the position of proton points in the same direction as $\vec{B}_0$ and thus decreases $\vec{B}_{induced}$. The overall effect appears as deshielding of the proton by fluorine. In contrast, when the molecular axis is parallel to $\vec{B}_0$ (Figure 2.4b) the electron shell of fluorine shields the proton.

In solutions, however, fast molecular motions and reorientations average out the chemical shielding to the isotropic value. More about the orientation dependence of the chemical shifts is given in the following section.

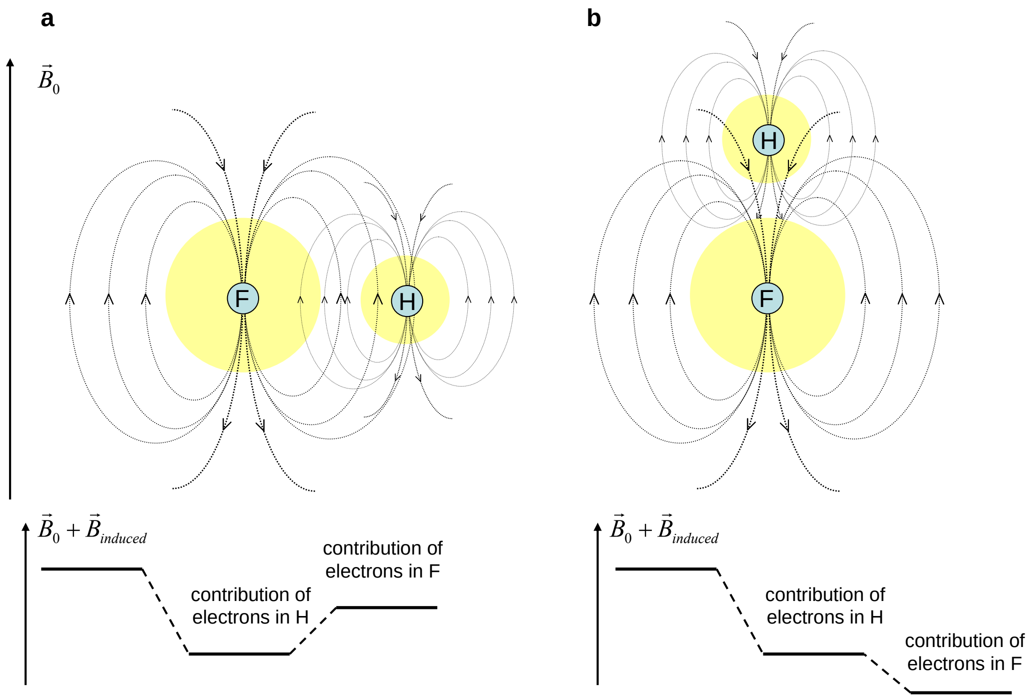

Figure 2.4. Orientational dependence of the ^{1}H chemical shift of FH molecule. (a) Deshielding of proton by the electron cloud of fluorine if the molecular axis is perpendicular to $\vec{B}_0$. (b) Shielding of proton by the electron cloud of fluorine if the molecular axis is parallel to $\vec{B}_0$.

2.3. Chemical shift anisotropy

In the previous section it has been shown that the nuclear shielding is a second rank tensor and can be represented by the 3x3 matrix. For a given orientation of the molecule in the laboratory frame (*xyz*) it can be written as

$$\sigma = \begin{pmatrix} \sigma_{xx} & \sigma_{xy} & \sigma_{xz} \\ \sigma_{yx} & \sigma_{yy} & \sigma_{yz} \\ \sigma_{zx} & \sigma_{zy} & \sigma_{zz} \end{pmatrix}. \quad (2.7)$$

Thus the magnetic field $\vec{B}$, experienced by the nucleus, equals to

$$\vec{B} = \vec{B}_0 + \vec{B}_{induced} = \vec{B}_0 - \sigma \cdot \vec{B}_0 = \begin{pmatrix} 0 \\ 0 \\ B_0 \end{pmatrix} - \begin{pmatrix} \sigma_{xx} & \sigma_{xy} & \sigma_{xz} \\ \sigma_{yx} & \sigma_{yy} & \sigma_{yz} \\ \sigma_{zx} & \sigma_{zy} & \sigma_{zz} \end{pmatrix} \cdot \begin{pmatrix} 0 \\ 0 \\ B_0 \end{pmatrix} = \begin{pmatrix} \sigma_{xz} B_0 \\ \sigma_{yz} B_0 \\ (1 - \sigma_{zz}) B_0 \end{pmatrix}. \quad (2.8)$$

Equation (2.8) shows that magnetic field $\vec{B}$ it not necessarily parallel to $\vec{B}_0$ and has components in all directions in the laboratory frame. This has the following consequence. If the molecule rotates with the Larmor frequency ω_0, the magnetic field $\vec{B}$ has the components perpendicular to $\vec{B}_0$, which tumble with the same frequency. This has an analogous effect on the nucleus as the radio-frequency pulse and results in faster T_1 relaxation.

It is always possible to find the so called *principal axis system* of the molecule (*XYZ*) in which chemical shielding tensor simplifies to

$$\sigma = \begin{pmatrix} \sigma_{XX} & 0 & 0 \\ 0 & \sigma_{YY} & 0 \\ 0 & 0 & \sigma_{ZZ} \end{pmatrix}. \quad (2.9)$$

The principal axes system is fixed to the molecule and moves together with it. Equation (2.9) means that if the molecule is oriented with one of its principal axes parallel to $\vec{B}_0$, the induced field $\vec{B}_{induced}$ is created only is this direction.

Consider now an arbitrary orientation of the molecule. The orientation of $\vec{B}_0$ with respect to the principal axis system can be defined by the angles θ_X, θ_Y and θ_Z between $\vec{B}_0$ and *X*, *Y* and *Z* axes. This is illustrated in Figure 2.5.

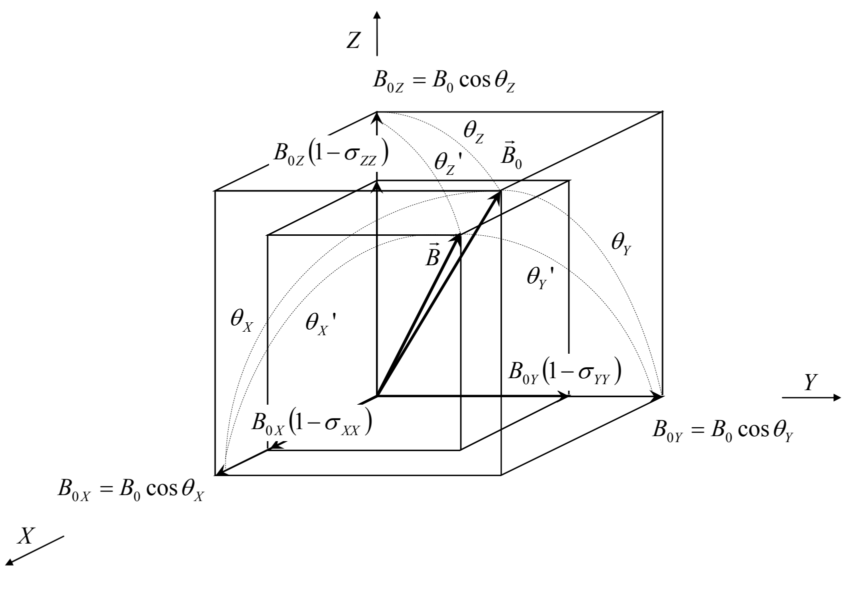

Figure 2.5. Projections of $\vec{B}_0$ and $\vec{B}$ on the principal axes system of the shielding tensor.

The projections of the $\vec{B}_0$ on X, Y and Z axes are given by

$$B_{0X} = B_0 \cos\theta_X,$$
$$B_{0Y} = B_0 \cos\theta_Y, \tag{2.10}$$
$$B_{0Z} = B_0 \cos\theta_Z.$$

According to (2.3) the projections of $\vec{B}$ on the principal axes are

$$B_X = (1-\sigma_{XX})B_{0X} = (1-\sigma_{XX})B_0 \cos\theta_X,$$
$$B_Y = (1-\sigma_{YY})B_{0Y} = (1-\sigma_{YY})B_0 \cos\theta_Y, \tag{2.11}$$
$$B_Z = (1-\sigma_{ZZ})B_{0Z} = (1-\sigma_{ZZ})B_0 \cos\theta_Z.$$

Projections of $\vec{B}$ are also shown in Figure 2.5. If we define the angles between $\vec{B}$ and principal axes as θ_X', θ_Y' and θ_Z' we get for the overall length of the vector $\vec{B}$:

$$\left|\vec{B}\right| = (1-\sigma_{XX})B_0 \cos\theta_X \cos\theta_X' + (1-\sigma_{YY})B_0 \cos\theta_Y \cos\theta_Y' + (1-\sigma_{ZZ})B_0 \cos\theta_Z \cos\theta_Z'. \tag{2.12}$$

For simplicity we make the *secular approximation* $\theta_X = \theta_X'$, $\theta_Y = \theta_Y'$ and $\theta_Z = \theta_Z'$, which allows to re-write (2.12) as

$$\left|\vec{B}\right| = (1-\sigma_{XX})B_0 \cos^2\theta_X + (1-\sigma_{YY})B_0 \cos^2\theta_Y + (1-\sigma_{ZZ})B_0 \cos^2\theta_Z. \tag{2.13}$$

Using the trigonometric equation

$$\cos^2\theta_X + \cos^2\theta_Y + \cos^2\theta_Z = 1 \tag{2.14}$$

we get

$$\left|\vec{B}\right| = B_0\left(1-\sigma_{XX}\cos^2\theta_X - \sigma_{YY}\cos^2\theta_Y - \sigma_{ZZ}\cos^2\theta_Z\right). \tag{2.15}$$

In other words, the effective shielding, experienced by the nucleus is given by

$$\sigma = \sigma_{XX}\cos^2\theta_X + \sigma_{YY}\cos^2\theta_Y + \sigma_{ZZ}\cos^2\theta_Z. \tag{2.16}$$

To analyse (2.16) further we will consider two special cases: a) fast rotating molecules with arbitrary σ and b) non-rotating molecules with the axially symmetric σ.

a) If the molecule reorients fast, the shielding averages to

$$\langle\sigma\rangle = \sigma_{XX}\langle\cos^2\theta_X\rangle + \sigma_{YY}\langle\cos^2\theta_Y\rangle + \sigma_{ZZ}\langle\cos^2\theta_Z\rangle. \tag{2.17}$$

If all the orientations of the molecule are equally probable,

$$\langle \cos^2\theta_X \rangle = \langle \cos^2\theta_Y \rangle = \langle \cos^2\theta_Z \rangle = \frac{1}{3} \quad (2.18)$$

and we get the isotropic shielding

$$\langle \sigma \rangle = \sigma_{iso} = \frac{1}{3}(\sigma_{XX} + \sigma_{YY} + \sigma_{ZZ}). \quad (2.19)$$

This value of shielding appears in the liquid-state NMR spectra.

b) Now consider non-rotating molecules with the axially symmetric tensor σ. We define

$$\sigma_\perp = \sigma_{XX} = \sigma_{YY},\ \sigma_\parallel = \sigma_{ZZ} \text{ and } \Delta\sigma = \sigma_\parallel - \sigma_\perp . \quad (2.20)$$

Equation (2.16) is then re-written as

$$\begin{aligned} \sigma &= \sigma_\perp(\cos^2\theta_X + \cos^2\theta_Y) + \sigma_\parallel \cos^2\theta_Z = \sigma_\perp(1 - \cos^2\theta_Z) + \sigma_\parallel \cos^2\theta_Z = \\ &\sigma_\perp + (\sigma_\parallel - \sigma_\perp)\cos^2\theta_Z = \sigma_\perp + \Delta\sigma \cos^2\theta_Z . \end{aligned} \quad (2.21)$$

Re-organization of (2.21) gives

$$\sigma = \sigma_\perp + \Delta\sigma\cos^2\theta_Z - \frac{\Delta\sigma}{3} + \frac{\Delta\sigma}{3} = \sigma_{aniso} + \sigma_\perp + \frac{1}{3}(\sigma_\parallel - \sigma_\perp) \quad (2.22)$$

or

$$\sigma = \sigma_{aniso} + \sigma_{iso}, \quad (2.23)$$

where

$$\sigma_{aniso} = \frac{\Delta\sigma}{3}(3\cos^2\theta_Z - 1) \text{ and } \sigma_{iso} = \frac{1}{3}(\sigma_\parallel + 2\sigma_\perp). \quad (2.24)$$

In other words, the shielding is the sum of the orientation-independent σ_{iso} and σ_{aniso}, which depends on the angle between $\vec{B}_0$ and the Z principal axis of the molecule. Orientation dependence of the shielding is called *chemical shift anisotropy*, or *CSA*.

Let us consider the spectral lineshapes created by CSA in the polycrystalline sample, which contains the powder of randomly oriented tiny crystals. The orientation of each crystal can be depicted as a point on a sphere (Figure 2.6a). If all the orientations are equally probable, the density of the points on the sphere is constant. However, there are more chances to be almost perpendicular to $\vec{B}_0$ than to be almost parallel to it. Thus the probability density P of finding the orientation with θ_Z is proportional to the sine of the angle:

$$P(\theta_Z) \propto \sin\theta_Z\,. \tag{2.25}$$

Each molecule contributes equally to the spectrum and the typical overall lineshape due to the chemical shift anisotropy is given at the bottom of Figure 2.7. It can be seen that the chemical shift anisotropy parameter $\Delta\sigma$ determines the width of the spectral signal. However, for very symmetric electron distribution, such as for the ^{15}N nucleus in NH_4^+ cation, the chemical shift anisotropy is zero.

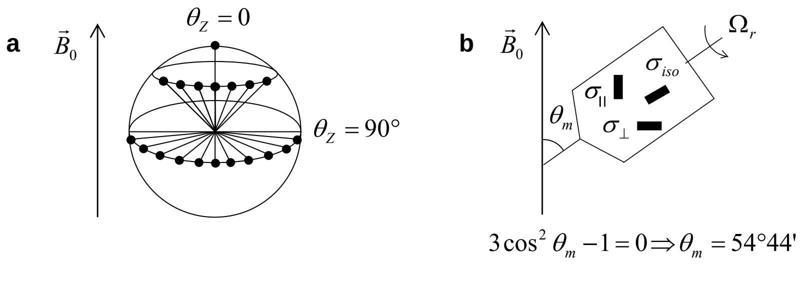

Figure 2.6. (a) distribution of molecular orientations in the polycrystalline (powdered) sample. (b) Orientation of the sample for the magic angle spinning (MAS), which leads to the cancellation of the CSA.

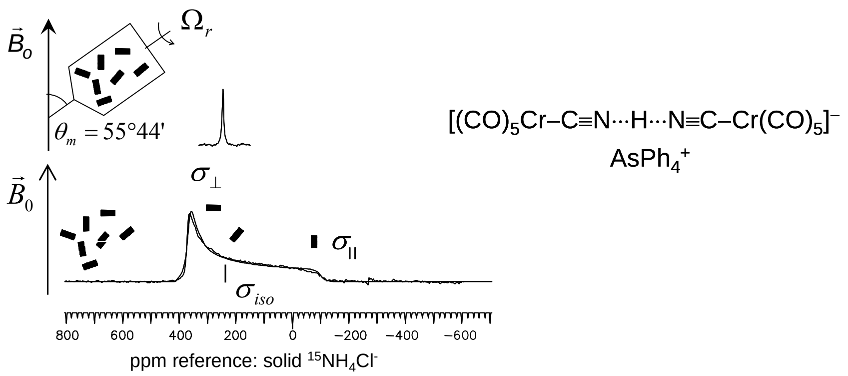

Figure 2.7. (bottom) Typical lineshape of the ^{15}N NMR signal determined by the chemical shift anisotropy; (top) the lineshape of the same ^{15}N NMR signal measured under the MAS condition. Adapted from H.Benedict, H.H.Limbach, M. Wehlan, W. P. Fehlhammer, N. S. Golubev, R. Janoschek, *J. Am. Chem. Soc.* **1998**, *120*, 2939.

Chemical shift anisotropy reflects the structure of the molecule. Consider, for example, the series of 1:1 hydrogen bonded complexes, formed between 2,4,6-trimethylpyridine and benzoic acids, shown in the left part of Figure 2.8. When the proton donating ability of the acid increases, the bridging proton shifts towards the nitrogen atom of pyridine. This proton shift changes the components of the ^{15}N shielding tensor, which is reflected in static NMR spectra.

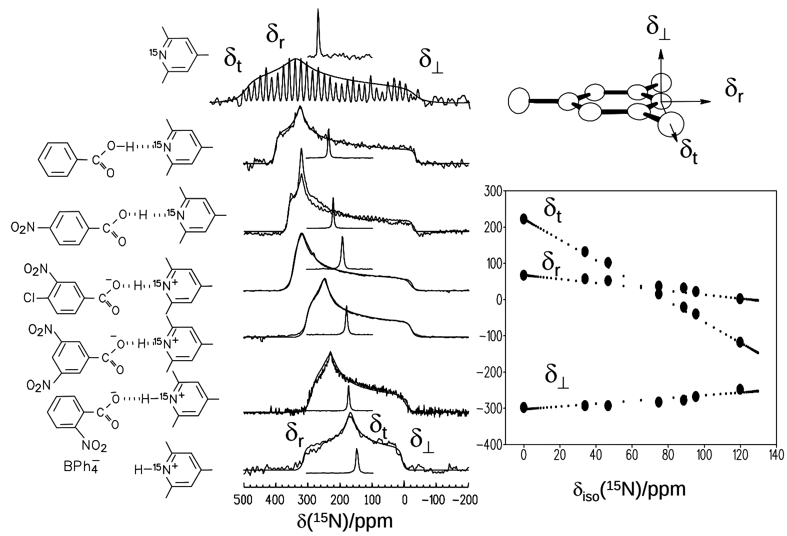

Figure 2.8. Static ^{15}N NMR spectra of 1:1 hydrogen bonded complexes, formed between 2,4,6-trimethylpyridine and series of benzoic acids. The isotropic signal, obtained under the MAS conditions is also shown. Adapted from Ph. Lorente, I.G.Shenderovich, G.Buntkowsky, N.S.Golubev, G.S.Denisov, H.H. Limbach, *Magn. Reson. Chem.* **2001,** *39*, S18.

2.4. Magic angle spinning

From (2.24) it follows that the anisotropic part of the chemical shielding tensor is cancelled is the molecule is oriented with the angle θ_Z determined by the equation

$$3\cos^2\theta_Z - 1 = 0 \Rightarrow \cos\theta_Z = \sqrt{\frac{1}{3}} \Rightarrow \theta_Z = 54°44' \ (54.7°). \qquad (2.26)$$

The angle $54°44'$ is called *magic angle*. If the crystal will be fast rotated with frequency Ω_r around the axis having magic angle with $\vec{B}_0$ (Figure 2.6b) all components of the shielding tensor which are not parallel to that axis will be averaged out. As a result, the anisotropic part of the shielding tensor will be cancelled and on the spectrum a sharp signal will be visible, exhibiting the shielding σ_{iso}. In other words, the spectrum will resemble the spectrum of the solution (see, for instance, upper spectrum in Figure 2.7 or sharp lines in Figure 2.8).

The *magic angle spinning* (*MAS*) technique is widely used in the solid-state NMR spectroscopy. Practically, the powder is usually placed inside the cylindrical rotor made of hard material withstanding significant centrifugal forces. The rotor is placed inside stator, around which the NMR coil is wrapped as a solenoid. Then the rotor is rotated by the gas flow with the typical frequencies from Ω_r = 5 kHz to Ω_r = 30 kHz. The up to date maximal commercially available MAS frequency is about 70 kHz. In order to understand why one needs high frequencies of MAS, consider the evolution of the anisotropic NMR signal upon increase of Ω_r, illustrated in Figure 2.9, which is given here without derivation.

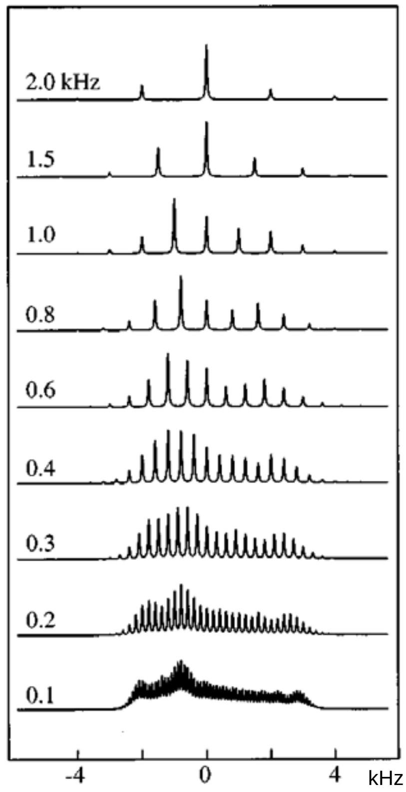

Figure 2.9. Simulated solid-state NMR spectra as a function of the frequency of MAS, Ω_r. Chemical shift tensor parameters are as follows: $\sigma_{XX} = -2.25$ kHz, $\sigma_{YY} = -0.75$ kHz, $\sigma_{ZZ} = 3$ kHz. Adapted from P. Hodgkinson, L. Emsley, *J. Chem. Phys.* **1997**, *107*, 4808.

It can be seen that the anisotropic lineshape is "modulated" by the rotational frequency and looks like a series of equidistant sharp lines, separated by Ω_r. Only when Ω_r is high enough the most intensive line in the spectrum corresponds to σ_{iso} and other lines, called "*rotational sidebands*" are weak and far away from the central line.

Fast rotational diffusion leads to effects similar to those of the MAS. This is illustrated in Figure 2.10. Bottom left spectrum shows the broad signal from a static sample. MAS of this sample leads to the sharp line shown in the bottom right spectrum. If the rotational diffusion is fast (top left) MAS will not lead to additional sharpening of the sample (top right). For the intermediate frequencies of rotational diffusion the line is homogenously broadened and MAS will not sharpen it. Homogenious broadening is due to the fast relaxation, because of the coincidence between rotational diffusion and Larmor frequencies.

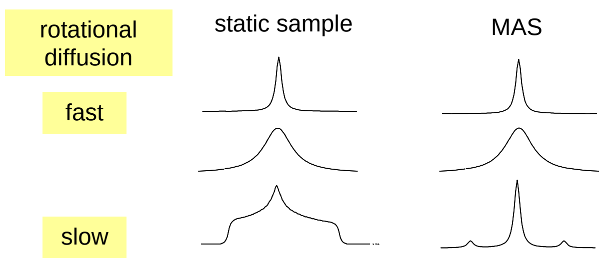

Figure 2.10. Effect of the rotational diffusion and MAS on the lineshape of the NMR signal.

Example of the rotational diffusion effect on the ^{13}C NMR signal of C_{60} is shown in Figure 2.11.

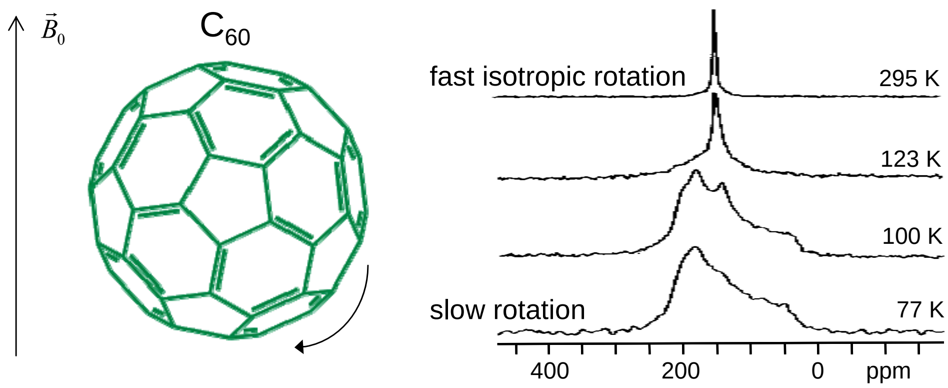

Figure 2.11. Rotational diffusion effects the shape of the ^{13}C NMR line of C_{60}. Adapted from C.S.Yannoni, R.D.Johnson, G.Meijer, D.S.Bethune, J.R.Salem *J. Phys.Chem.*, **1991**, *95*, 9.

2.5. Effect of intramolecular rotations on ^{1}H chemical shifts.

Consider the XRR'C-CH$_a$H$_b$Y molecule. We will demonstrate that even in case of fast intramolecular rotation around the C-C bond (tautomerism between three rotamers) protons H$_a$ and H$_b$ are chemically non-equivalent. The Newman projections of the three rotamers of the molecule are shown in Figure 2.12. Rotamers are labelled 1, 2 and 3.

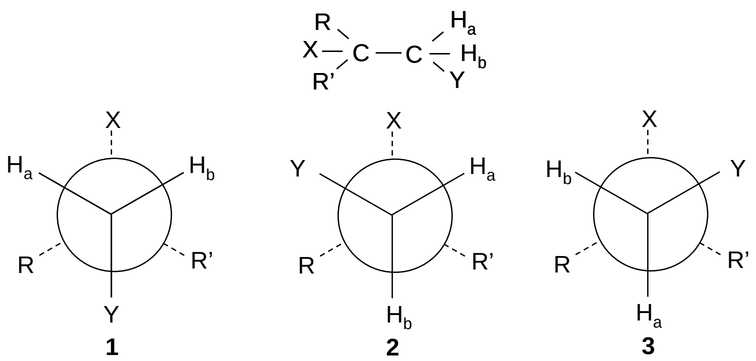

Figure 2.12. Newman projections of three rotamers of the XRR'C-CH$_a$H$_b$Y molecule.

The fractions of rotamers are given by x_1, x_2 and x_3. In the NMR experiment the averaged NMR parameters will be observed, weighted with the fractions of rotamers. For chemical shifts of H$_a$ and H$_b$ protons we get

$$\begin{aligned}\delta_a &= x_1\delta_{a1} + x_2\delta_{a2} + x_3\delta_{a3} \\ \delta_b &= x_1\delta_{b1} + x_2\delta_{b2} + x_3\delta_{b3}\end{aligned}. \qquad (2.27)$$

Let us assume that R = R'. In this case the following equations hold:

$$x_2 = x_3,$$
$$\delta_{a1} = \delta_{b1},$$
$$\delta_{a2} = \delta_{b3}, \tag{2.28}$$
$$\delta_{b2} = \delta_{a3}.$$

Using (2.28), equations (2.27) can be re-written as

$$\begin{aligned} \delta_a &= x_1\delta_{a1} + x_2(\delta_{a2} + \delta_{a3}) \\ \delta_b &= x_1\delta_{b1} + x_2(\delta_{b2} + \delta_{b3}) \end{aligned}. \tag{2.29}$$

Finally,

$$\begin{aligned} \delta_a &= x_1\delta_{a1} + x_2(\delta_{a2} + \delta_{a3}) \\ \delta_b &= x_1\delta_{b1} + x_2(\delta_{a3} + \delta_{a2}) \end{aligned}. \tag{2.30}$$

Thus, if R = R' then $\delta_a = \delta_b$. In case if R $\neq$ R' the simplification of (2.27) is not possible and $\delta_a \neq \delta_b$. In other words, methylene protons adjacent to the chiral carbon atom are chemically non-equivalent. The example is shown in Figure 2.13 for $(CH_3)ClHC\text{-}CH_aH_bCl$ molecule dissolved in $CDCl_3$.

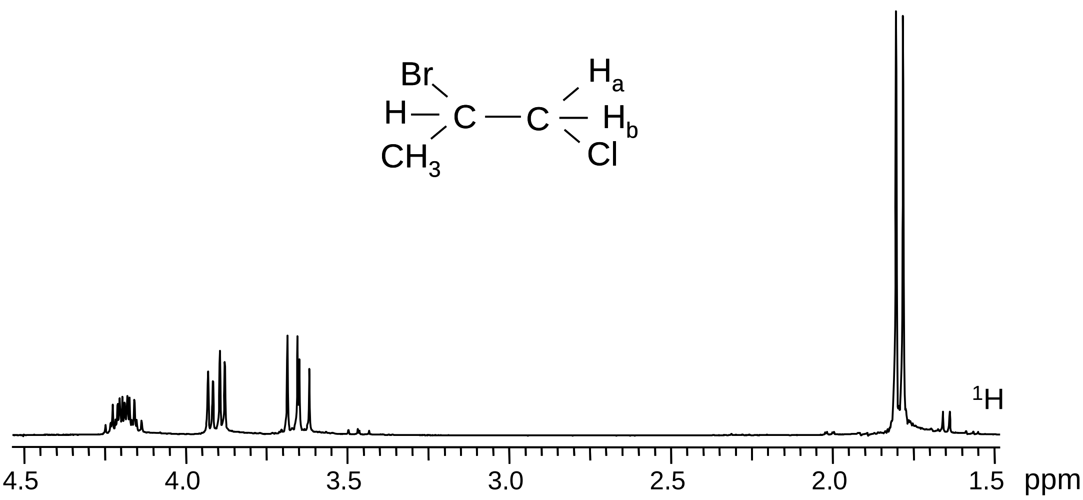

Figure 2.13. ^1H NMR spectrum of $(CH_3)ClHC\text{-}CH_aH_bCl$ dissolved in $CDCl_3$.

3. Dipolar interaction

3.1. Classical dipolar interaction

Consider two magnetic dipoles, $\vec{\mu}_1$ and $\vec{\mu}_2$, arbitrary oriented in space at a distance $\vec{r}$ between them. Different orientations of one dipole in the magnetic field created by the other have different energies, according to (1.4). In can be demonstrated – though in this course it is given without derivation – that the energy of interaction of two magnetic dipoles (in cgs system) is given by

$$E_d = \frac{\vec{\mu}_1 \cdot \vec{\mu}_1}{r^3} - 3\frac{(\vec{\mu}_1 \cdot \vec{r})(\vec{\mu}_2 \cdot \vec{r})}{r^5}. \tag{3.1}$$

Equation (3.1) can be re-written as

$$E_d = \frac{\mu_1 \mu_2}{r^3}(\cos\alpha - 3\cos\beta\cos\gamma), \tag{3.2}$$

where μ_1 and μ_2 are absolute values of $\vec{\mu}_1$ and $\vec{\mu}_2$; α is the angle between $\vec{\mu}_1$ and $\vec{\mu}_2$; β is the angle between $\vec{\mu}_1$ and $\vec{r}$; γ is the angle between $\vec{\mu}_2$ and $\vec{r}$. In order to demonstrate the dependence of E_d on α, β and γ let us consider the interaction energy in several special cases, illustrated in Figure 3.1. At the bottom of the Figure the values of the interaction energy E_d are given.

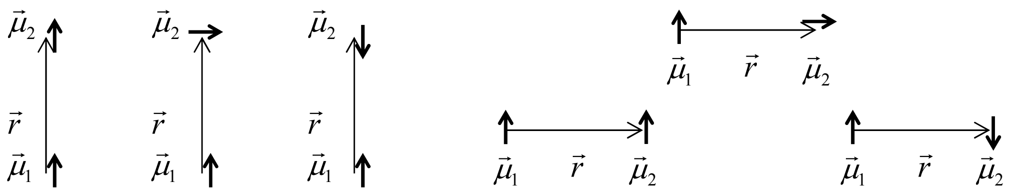

	$\alpha = 0°$	$\alpha = 90°$	$\alpha = 180°$	$\alpha = 0°$	$\alpha = 90°$	$\alpha = 180°$
	$\beta = 0°$	$\beta = 0°$	$\beta = 0°$	$\beta = 90°$	$\beta = 90°$	$\beta = 90°$
	$\gamma = 0°$	$\gamma = 90°$	$\gamma = 180°$	$\gamma = 90°$	$\gamma = 0°$	$\gamma = 90°$
$E_d =$	$-2\frac{\lvert\vec{\mu}_1\rvert\lvert\vec{\mu}_2\rvert}{r^3}$	0	$+2\frac{\lvert\vec{\mu}_1\rvert\lvert\vec{\mu}_2\rvert}{r^3}$	$+\frac{\lvert\vec{\mu}_1\rvert\lvert\vec{\mu}_2\rvert}{r^3}$	0	$-\frac{\lvert\vec{\mu}_1\rvert\lvert\vec{\mu}_2\rvert}{r^3}$

Figure 3.1. Energy E_d of dipole-dipole interaction of magnetic dipoles $\vec{\mu}_1$ and $\vec{\mu}_2$ at distance $\vec{r}$ for selected mutual orientations.

It can be seen, that most stable orientations are reached when dipoles are parallel if they are "on top of each other" and when they are anti-parallel, if they are "side by side".

If dipoles $\vec{\mu}_1$ and $\vec{\mu}_2$ correspond to the nuclei with spins ½, only two orientations of each spin are allowed. Angle α can only be 0° or 180°. Furthermore, angles β and γ are related and can be expressed through angle θ between $\vec{r}$ and $\overline{B}_0$. In Figure 3.2 are shown all 4 possible spin states for an arbitrary angle θ. At the bottom are given the interaction energies E_d for each case.

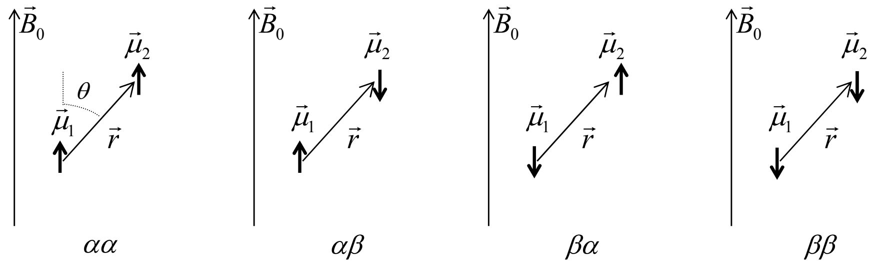

$\alpha = 0°$	$\alpha = 180°$	$\alpha = 180°$	$\alpha = 0°$
$\beta = \theta$	$\beta = \theta$	$\beta = 180° - \theta$	$\beta = 180° - \theta$
$\gamma = \theta$	$\gamma = 180° - \theta$	$\gamma = \theta$	$\gamma = 180° - \theta$
$E_d = \frac{\lvert\vec{\mu}_1\rvert\lvert\vec{\mu}_2\rvert}{r^3}\left(1 - 3\cos^2\theta\right)$	$E_d = -\frac{\lvert\vec{\mu}_1\rvert\lvert\vec{\mu}_2\rvert}{r^3}\left(1 - 3\cos^2\theta\right)$	$E_d = -\frac{\lvert\vec{\mu}_1\rvert\lvert\vec{\mu}_2\rvert}{r^3}\left(1 - 3\cos^2\theta\right)$	$E_d = \frac{\lvert\vec{\mu}_1\rvert\lvert\vec{\mu}_2\rvert}{r^3}\left(1 - 3\cos^2\theta\right)$

Figure 3.2. Energy E_d of dipole-dipole interaction of magnetic dipoles $\vec{\mu}_1$ and $\vec{\mu}_2$, which correspond to the nuclear spins 1/2 in the external magnetic field $\vec{B}_0$. θ is the angle between $\vec{B}_0$ and the vector $\vec{r}$, connecting two dipole moments.

Taking into account that

$$\mu_{iz} = m_i \gamma_i \hbar, \tag{3.3}$$

where i = 1, 2, the expressions for E_d can be simplified to a single one:

$$E_d = \frac{\mu_{1z}\mu_{2z}}{r^3}\left(1 - 3\cos^2\theta\right) = m_1 m_2 \frac{\gamma_1\gamma_2}{r^3}\hbar^2\left(1 - 3\cos^2\theta\right) = m_1 m_2 J_d, \tag{3.4}$$

where

$$J_d = D\left(1 - 3\cos^2\theta\right) \text{ and } D = \frac{\gamma_1\gamma_2}{r^3}\hbar^2. \tag{3.5}$$

J_d is orientation-dependent *dipolar splitting* and D is orientation-independent *dipolar coupling constant*. Dipolar coupling constant depends on the gyromagnetic ratios of interacting nuclei and falls with the distance as $\frac{1}{r^3}$.

Expression (3.5) is valid in cgs system. In SI one obtains $D = \frac{\mu_0}{4\pi}\frac{\gamma_1\gamma_2}{r^3}\hbar^2$, where magnetic permeability of the vacuum $\mu_0 = 4\pi \cdot 10^{-7}$ [Vs/Am]. For the expression of the dipolar coupling constant in frequency units, the corresponding expressions in cgs and SI have to be divided by Planck's constant h.

For example, let us calculate the dipolar coupling constant of two proton separated by the distance r:

$$D^{HH} = 10^{-7}\,\frac{26.7\cdot 10^{7}\cdot 26.7\cdot 10^{7}}{r^{3}}\cdot\frac{6.626\cdot 10^{-34}}{(2\cdot 3.14)^{2}} \approx \frac{1.2\cdot 10^{-25}}{r^{3}}\ \text{[Hz]} \tag{3.6}$$

or

$$D^{HH} \approx \frac{120}{r^{3}}\ \text{[kHz]} \tag{3.7}$$

if the distance r is in Angstroms.

3.2. Quantum-mechanical description of dipolar coupled two-spin system.

Before we consider the system of two dipolar-coupled spins in the external magnetic field, let us review the basic quantum-mechanical description of a single spin 1/2. This description was given in Chapter 1 and it is repeated here in a more compact form, which will be convenient later to describe the dipolar-coupled spin system. Hamilton operator for a single spin is given by

$$\hat{H} = -B_0\hat{\mu}_z = -\gamma B_0 \hat{I}_z\,, \tag{3.8}$$

where angular momentum operator $\hat{I}_z$ is defined through its action of the spin wave functions:

$$\hat{I}_z|\alpha\rangle = \frac{1}{2}\hbar|\alpha\rangle \text{ and}$$
$$\hat{I}_z|\beta\rangle = -\frac{1}{2}\hbar|\beta\rangle\,. \tag{3.9}$$

Energy levels, corresponding to the spin states $|\alpha\rangle$ and $|\beta\rangle$ can be found as the expectation values of the hamiltonian:

$$E_\alpha = \langle\alpha|\hat{H}|\alpha\rangle = \langle\alpha|-\gamma B_0\hat{I}_z|\alpha\rangle = \langle\alpha|-\gamma B_0\frac{1}{2}\hbar|\alpha\rangle = -\gamma B_0\frac{1}{2}\hbar = -\frac{1}{2}h\nu \text{ and}$$
$$E_\beta = \langle\beta|\hat{H}|\beta\rangle = \langle\beta|-\gamma B_0\hat{I}_z|\beta\rangle = \langle\beta|\gamma B_0\frac{1}{2}\hbar|\beta\rangle = \gamma B_0\frac{1}{2}\hbar = \frac{1}{2}h\nu\,. \tag{3.10}$$

In the frequency units we get

$$E_\alpha = -\frac{1}{2}\nu \text{ and } E_\beta = \frac{1}{2}\nu\,. \tag{3.11}$$

Now we come to the dipolar-coupled two-spin system. We assume nuclei to be different (heteronuclear case) and both of them having spin 1/2. In this case the four possible spin states can then be expressed as Zeeman products:

$$\left|\alpha\alpha\right\rangle \equiv 1, \left|\alpha\beta\right\rangle \equiv 2, \left|\beta\alpha\right\rangle \equiv 3, \left|\beta\beta\right\rangle \equiv 4 . \tag{3.12}$$

Spin states are numbered 1-4 to make the nomenclature more compact.

> Homonuclear coupling would lead to the mixing of the Zeeman product states and thus to the more complex expressions for the energy and spin wave functions. Homonuclear dipolar coupling case will not be considered in detail in this course. More about the mixing of Zeeman states of two interacting spins will be given in the Chapter "Scalar coupling".

Hamilton operator for the two-spin system can be constructed using the expression (3.4) and (3.8):

$$\hat{H} = -\gamma_1 B_0 \hat{I}_{1z} - \gamma_2 B_0 \hat{I}_{2z} + \frac{\gamma_1\gamma_2}{r^3}\left(1-3\cos^2\theta\right)\hat{I}_{1z}\hat{I}_{2z} . \tag{3.13}$$

Energy states, corresponding to spin states (3.12) and Hamilton operator (3.13) are as follows:

$$\begin{gathered} E_{\alpha\alpha} \equiv E_1 = \left\langle\alpha\alpha\right|\hat{H}\left|\alpha\alpha\right\rangle = \left\langle\alpha\alpha\right| -\gamma_1 B_0 \hat{I}_{1z}\left|\alpha\alpha\right\rangle + \left\langle\alpha\alpha\right| -\gamma_2 B_0 \hat{I}_{2z}\left|\alpha\alpha\right\rangle + \\ \left\langle\alpha\alpha\right|\frac{\gamma_1\gamma_2}{r^3}\left(1-3\cos^2\theta\right)\hat{I}_{1z}\hat{I}_{2z}\left|\alpha\alpha\right\rangle = -\gamma_1 B_0\frac{1}{2}\hbar\left\langle\alpha\alpha\middle|\alpha\alpha\right\rangle - \gamma_2 B_0 \frac{1}{2}\hbar\left\langle\alpha\alpha\middle|\alpha\alpha\right\rangle + . \\ \frac{\gamma_1\gamma_2}{r^3}\left(1-3\cos^2\theta\right)\frac{1}{2}\hbar\frac{1}{2}\hbar\left\langle\alpha\alpha\middle|\alpha\alpha\right\rangle = -\frac{1}{2}h\nu_1 - \frac{1}{2}h\nu_2 + \frac{1}{4}J_d \end{gathered} \tag{3.14}$$

In the similar way we get

$$E_{\alpha\beta} \equiv E_2 = \left\langle\alpha\beta\right|\hat{H}\left|\alpha\beta\right\rangle = -\frac{1}{2}h\nu_1 + \frac{1}{2}h\nu_2 - \frac{1}{4}J_d . \tag{3.15}$$

$$E_{\beta\alpha} \equiv E_3 = \left\langle\beta\alpha\right|\hat{H}\left|\beta\alpha\right\rangle = +\frac{1}{2}h\nu_1 - \frac{1}{2}h\nu_2 - \frac{1}{4}J_d \tag{3.16}$$

and

$$E_{\beta\beta} \equiv E_4 = \left\langle\beta\beta\right|\hat{H}\left|\beta\beta\right\rangle = +\frac{1}{2}h\nu_1 + \frac{1}{2}h\nu_2 + \frac{1}{4}J_d \tag{3.17}$$

Expressions (3.14)-(3.17) show that the dipolar coupling leads to the shift of the energy levels. As the dipolar splitting J_d is orientation-dependent, this shift depends on the orientation of the molecule with respect to the external magnetic field. In Figure 3.3 the position of the energy levels is shown as a function of the angle θ between $\vec{B}_0$ and the radius vector $\vec{r}$, connecting two spins. At $\theta = 0°$ each energy level is shifted by the absolute value $2D$ and at $\theta = 90°$ by the absolute value D. At the magic angle $\theta = 54°44'$ the energy levels coincide with those obtained for non-coupled pair of spins.

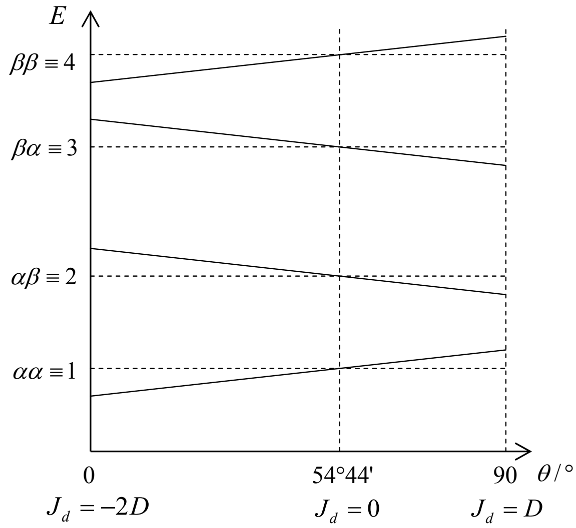

Figure 3.3. Energy level diagram for the dipolar-coupled two-spin system as a function of the angle θ between $\vec{B}_0$ and the radius vector $\vec{r}$, connecting two spins.

Now we consider the possible transition between these energy levels. For simplicity, we will consider only three values of the angle θ: $0°$, $54°44'$ and $90°$, illustrated in Figure 3.4. The allowed spin transitions are shown as vertical arrows and the corresponding frequencies are shown in the bottom of the Figure. For example, for the first nucleus transitions $\alpha\alpha \to \beta\alpha$ and $\alpha\beta \to \beta\beta$ are allowed. For the $\theta = 0°$ orientation, the frequencies of these transitions do not coincide and two lines separated by $2D$ appear in the spectrum. For $\theta = 54°44'$ frequencies of $\alpha\alpha \to \beta\alpha$ and $\alpha\beta \to \beta\beta$ transitions coincide and only one line appears. Finally, for $\theta = 90°$ two lines appear, separated by D. The same reasoning is valid for the second nucleus, though the frequencies of transitions are different.

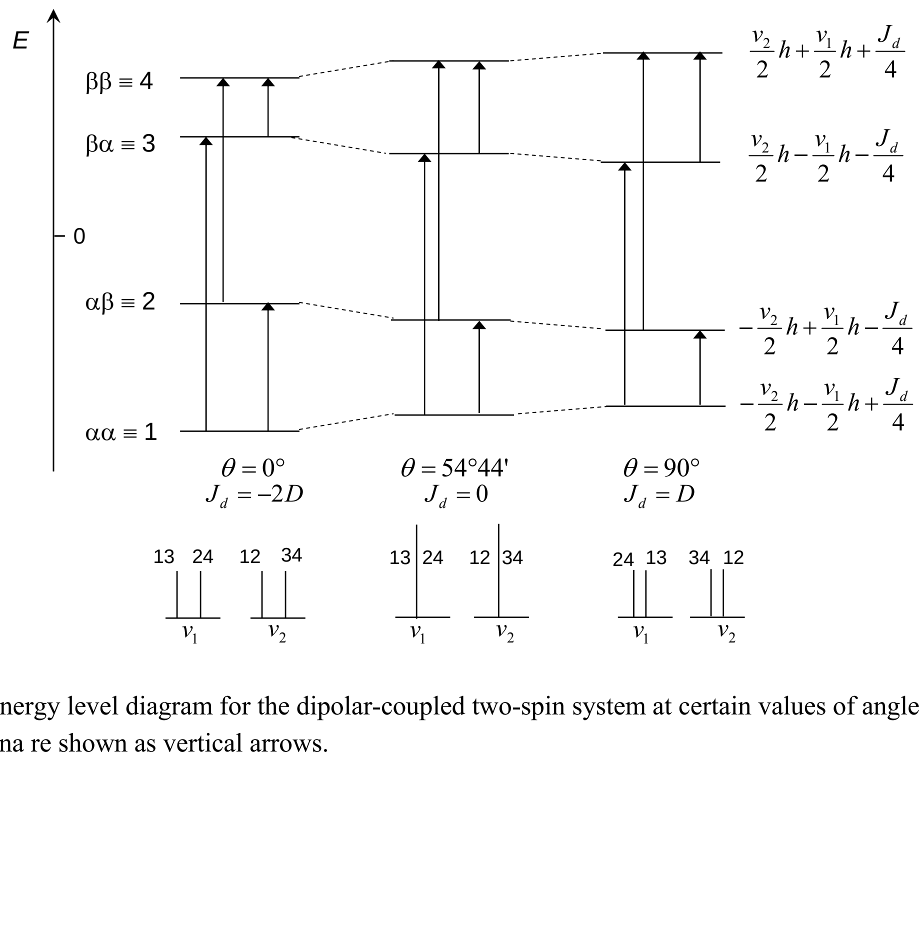

Figure 3.4. Energy level diagram for the dipolar-coupled two-spin system at certain values of angle θ. Allowed spin transitiona re shown as vertical arrows.

The probability to find molecules with certain value of θ is proportional to $\sin\theta$ (see (2.25) and Figure 2.6). Thus, for the powdered sample, consisting of many randomly oriented tiny crystals, in the spectrum of nucleus 1 we get the overall lineshape, illustrated in Figure 3.5. It is known as *Pake doublet* and it is an overlap of two signals, reflecting two possible spin states of nucleus 2. The spikes of the doublet are separated by D (in frequency units). The overall width of the signal is $2D$.

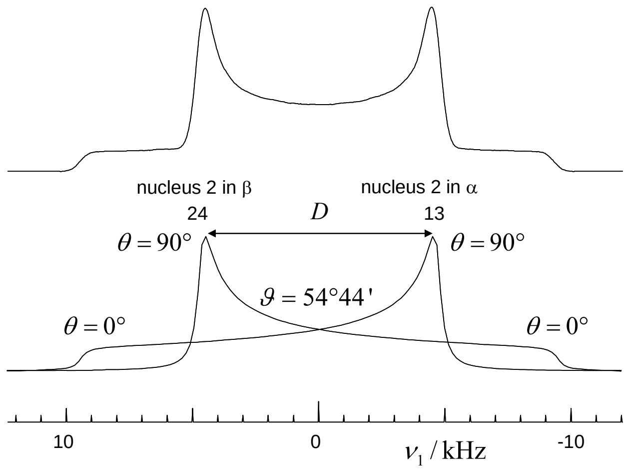

Figure 3.5. The Pake doublet lineshape due to the dipolar coupling of two spins ½ with positive gyromagnetic ratios. See text for more detail.

The parameter D, which can be directly measured from the NMR spectrum, is proportional to the average inverse cubic distance between dipolar-coupled spins, see (3.5). Thus, measurements of dipolar couplings allow one to estimate the interatomic distances in the molecules. Example of such measurements is shown in Figure 3.6.

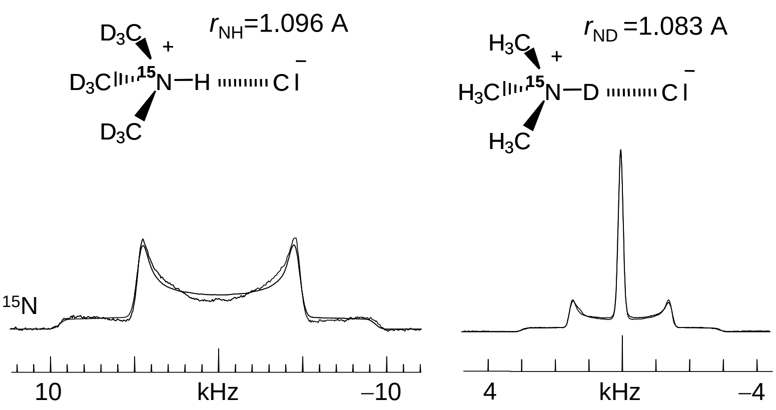

Figure 3.6. Estimation of the interatomic distances using the dipolar coupling constant. Ch. Hoelger, H.H.Limbach, *J. Phys.Chem.*, **1994**, *98*, 11803.

In the left-hand side of the Figure is shown the static ^{15}N NMR spectrum of $(CD_3)_3NH^+Cl^-$ salt. In this molecule the ^{15}N chemical shift anisotropy is very small due to high symmetry of the electron clouds around ^{15}N nucleus. Besides, due to the small gyromagnetic ratios of deuterons and relatively large distance to them, we can neglect the dipolar coupling between ^{15}N and 9 methyl deuterons. Thus the only remaining interaction is the dipolar coupling between ^{15}N and ^{1}H. Experimentally observed dipolar coupling constant corresponds to r_{NH} = 1.096 Å.

In the right-hand side of Figure 3.6 is shown the static ^{15}N NMR spectrum of $(CH_3)_3ND^+Cl^-$ salt. Special pulse sequence was used to remove the ^{15}N-^{1}H dipole-dipole interactions ("proton decoupling") and thus the only remaining interaction is the dipole coupling between ^{15}N and ^{2}H, which corresponded to the distance r_{ND} = 1.083 Å.

Note that interaction with deuteron, which has spin 1, leads to so called *Pake triplet*; we will not discuss this lineshape in detail in this course. Note also that $\gamma_{1H} \approx 6.5\gamma_{2H}$ and the resulting ^{15}N-^{2}H dipolar coupling constant is approximately 6.5 smaller than ^{15}N-^{1}H coupling constant. The deviations is due to the isotope effect on the average distance. The isotope effect gave $r_{ND} - r_{NH}$ = 0.016 Å is mainly due to the anharmonicity of the proton stretching vibration.

Magic angle spinning and molecular motions, such as rotational diffusion, affect the shape of the signal (Figure 3.7). While the Pake doublet is observed in the absence of motions (bottom left), fast molecular reorientations will average dipolar coupling to zero (top left). Under the magic angle spinning conditions (MAS) the dipolar coupling is also averaged out (bottom right) and further molecular motions will not affect the lineshape significantly (top right). In the intermediate cases the signal is homogenously broadened due to the fast relaxation, caused by the coincidence between rotational diffusion rate and dipolar coupling constant (middle left and right).

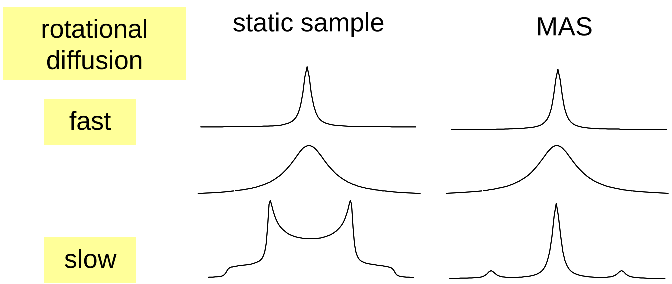

Figure 3.7. Effect of MAS and rotational diffusion on the lineshape of the signal of dipolar coupled two-spin system.

The differences between heteronuclear and homonuclear dipolar coupling can be demonstrated using Figure 3.8. At the bottom is shown static solid-state NMR spectrum of the system of two non-coupled nuclei: sharp signals at frequencies ν_1 and ν_2. In the presence of dipolar coupling both signals are split into the Pake doublets (AX spin system, $|\nu_1 - \nu_2| >> D$). When $|\nu_1 - \nu_2|$ becomes comparable to D, Pake doublets become distorted (AB spin system). This effect comes from the mixing of Zeeman product states and it is not unlike the roof effect in the liquid-state NMR spectra. In the limiting case of A_2 spin system, $|\nu_1 - \nu_2| << D$, the Pake doublet is split by $\frac{3}{2}D$ (given without derivation).

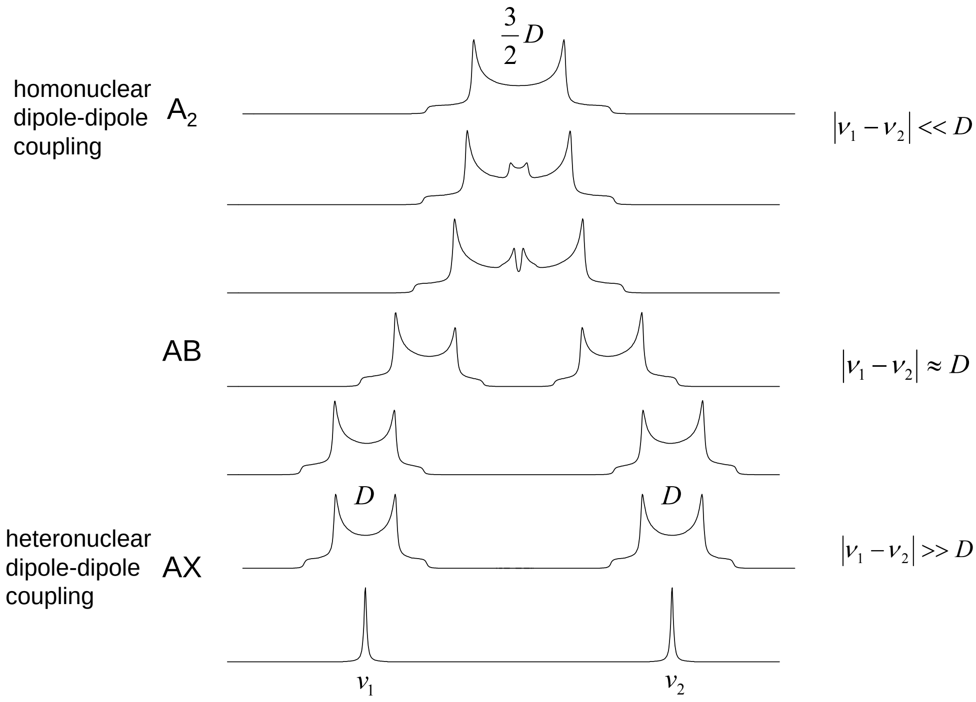

Figure 3.8. Transformation of the static spectra of an AX spin system of two dipolar coupled spins ½ into AB and eventually A_2 spin system.

3.3. Cross polarisation technique.

Nuclei such as ^{13}C and ^{15}N have rather low natural abundance (1.11% of ^{13}C and 0.37% of ^{15}N). Besides, these nuclei have relatively low gyromagnetic ratios and thus small Zeeman splitting of the energy levels, which leads to the small difference in their populations ($\gamma_{13C} = 67.3 \cdot 10^6$ $T^{-1}s^{-1}$, $\gamma_{15N} = -27.1 \cdot 10^6$ $T^{-1}s^{-1}$). All of this makes it complicated to acquire ^{13}C and ^{15}N NMR spectra with good signal-to-noise ratio. In general, ^{13}C, ^{15}N and similar nuclei are often referred to as *X nuclei* or *heavy nuclei*, though in the NMR spectroscopy the mass of the nucleus rarely plays an important role.

Cross polarisation (CP) is a pulse sequence which utilizes the dipolar coupling between X and neighbouring ^1H in order to increase the magnetisation of the X. Higher magnetisation results in more intensive NMR signal and in better signal-to-noise ratio. It is convenient to describe the CP pulse sequence in so called *doubly rotating frame*, in which ^1H are considered in the frame which rotates with the Larmor frequency of ^1H and X nuclei are considered in the rotating frame which rotates with the Larmor frequency of X. In such double rotating frame all the radio-frequency pulses appear static. The overview of the CP pulse sequence is given in Figure 3.9 and considered in more details below.

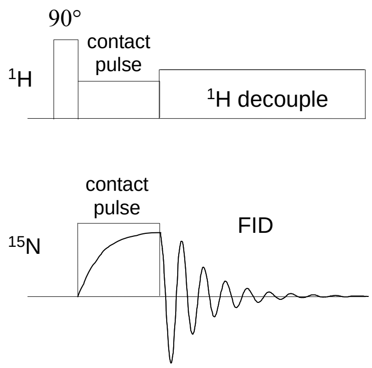

Figure 3.9. The overview of the cross polarisation pulse sequence.

Before the pulses the spin system is in equilibrium, i.e. the magnetisations $\vec{M}_H$ and $\vec{M}_X$ have their equilibrium values, corresponding to the strength of the external magnetic field $\vec{B}_0$ (see Figure 3.10, left). The magnetisation $\vec{M}_X$ is small and it is not sufficient for measurements of the spectrum. The CP sequence starts with the 90° pulse for ^{1}H. During the pulse the magnetisation $\vec{M}_H$ precesses around the direction of the magnetic field of the pulse, $\vec{B}_1^{-z}$, and after the pulse it is parallel to the υ axis of the rotating frame.

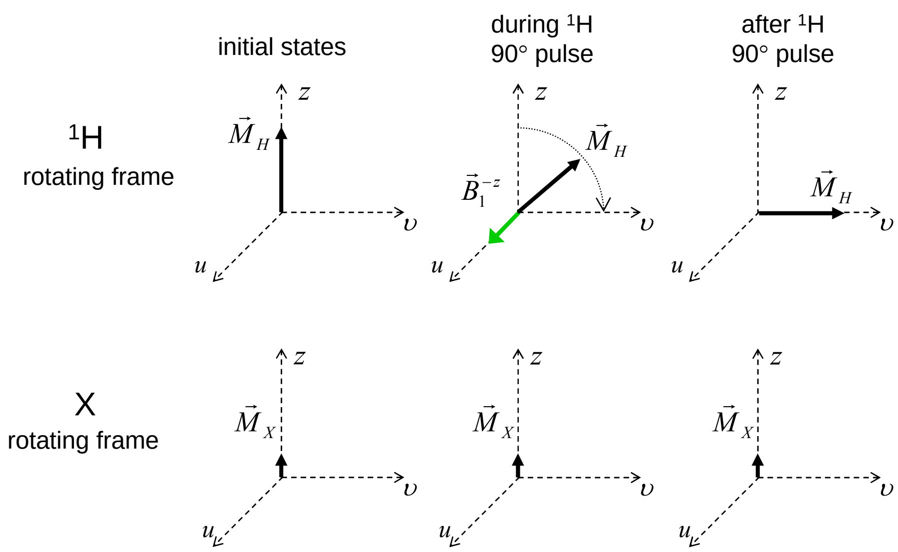

Figure 3.10. Time evolutions of magnetisations during the 90° pulse for ^{1}H, which precedes the contact pulse in the CP sequence.

After the 90° pulse so called *spin lock* pulse is applied for ^{1}H in υ direction (Figure 3.11, top left). It acts on the ^{1}H magnetisation in the rotating frame in the same way as $\vec{B}_0$ does in the laboratory frame: it maintains, to some extent, the magnetisation along the υ axis. In other words, the direction of the magnetic field of the pulse, $B_{1\upsilon}(H)$, serves as a new quantization axis for ^{1}H. Spin states corresponding to this axis are labelled as α_H^* and β_H^*. The Zeeman splitting of the corresponding energy levels is given by

$$\Delta E_H = \gamma_H B_{1\upsilon}(H). \tag{3.18}$$

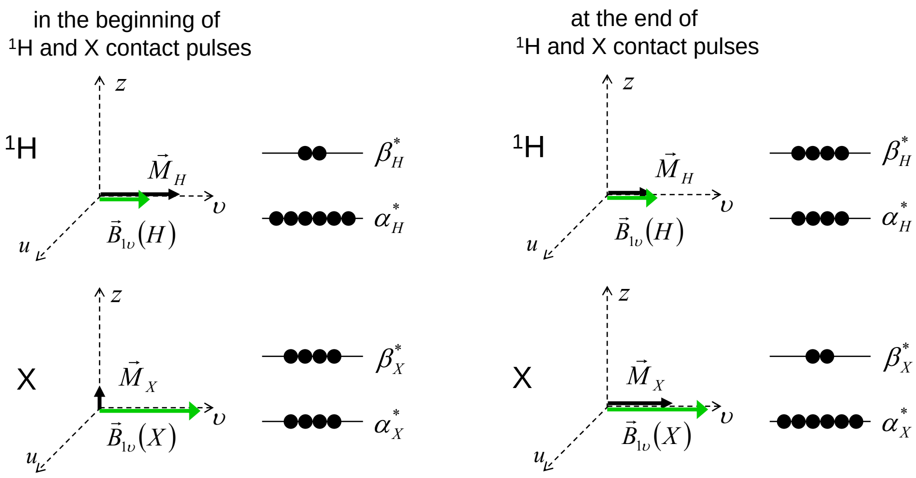

Figure 3.11. Time evolutions of magnetisations and energy level populations during the contact pulse in CP.

Similar contact pulse is simultaneously applied for X nuclei. It also serves as a new quantisation axis and splitting of energy levels α_X^* and β_X^* is given by

$$\Delta E_X = \gamma_X B_{1\upsilon}(X). \tag{3.19}$$

At the beginning of the contact pulse the population difference between α_H^* and β_H^* is big and that between α_X^* and β_X^* is zero. Using the average hamiltonian theory it is possible to show that during the contact pulse only those spin transitions are allowed which do not change both the energy and the angular momentum of the HX spin system. If one selects the intensities of the contact pulses so that

$$\Delta E_X = \Delta E_H \text{, i.e. } \gamma_X B_{1\upsilon}(X) = \gamma_H B_{1\upsilon}(H), \tag{3.20}$$

the redistribution of the energy is allowed which transfers the magnetisation from H to X. Equation (3.20) is called *Hartmann-Hahn condition*. As the intensity of the magnetic field $B_{1\upsilon}(H)$ is much smaller than intensity of $\vec{B}_0$, the magnetisation $\vec{M}_H$ decreases with time. Transitions from α_H^* to β_H^* are compensated by the transitions from β_X^* to α_X^* and the overall energy and angular momentum is conserved. At the end of the contact pulse the situation shown in the right part of Figure 3.11 is reached. Finally, the Free Induction Decay is recorded for X nuclei, while proton decoupling is usually applied in order to remove the HX dipole interaction. Cross polarisation is often used in combination with the magic angle spinning (CP MAS).

4. Scalar coupling

4.1. Origins of scalar coupling

Experiment shows that apart of dipole-dipole interaction there is a second type of coupling between nuclear spins, which is called *scalar coupling*. This type of interaction has no direct analogy in classical physics. Below we try to demonstrate its origins. Consider the hydrogen atom, consisting of proton and electron (Figure 4.1a). In classical description, two bodies can not share the same space. In reality, however, wavefunctions of the particles can overlap. As a result, there is certain probability density of finding the electron in the position of the nucleus. This is true for each electronic orbital, though for the *s*-orbitals it is significantly bigger than for *p*-, *d*- or higher orbitals (Figure 4.1b).

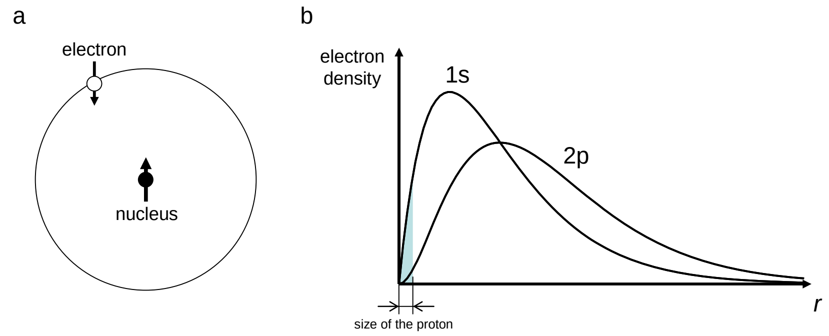

Figure 4.1. (a) Hydrogen atom in the electronic ground state. (b) Radial component of the electron density for the *s*- and *p*-orbitals of the hydrogen atom; probability to find the electron in the place of the nucleus is shown.

Electron and proton both have magnetic dipole moments and there is dipole-dipole interaction between them. This interaction is mostly averaged out to zero because the electron is delocalized on the orbital. The part of the dipole-dipole interaction which does not average to zero comes from the overlap of the electronic and nuclear wavefunctions. Roughly speaking, the contribution to the overall dipole-dipole interaction from each point of electron cloud is compensated by the contribution from the "opposite" point of the cloud, but for the electron density inside the nucleus there is no compensation. Thus, there is slight overall energetic preference for the magnetic dipoles of electron and nucleus to be anti-parallel, as schematically shown in Figure 4.1a. Consider now the H_2 molecule, depicted in Figure 4.2.

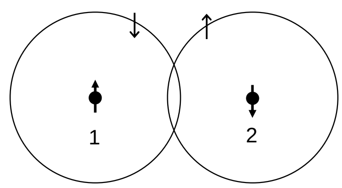

Figure 4.2. Scalar spin-spin coupling of two protons in H_2 molecule, mediated by the electrons.

For simplicity we show the molecular orbital as a sum of two atomic orbitals. Although in reality electrons are delocalized, there is a high probability that one electron is near nucleus 1 and other is near nucleus 2. We start our reasoning by looking at nucleus 1. The electron, which is close to nucleus 1 prefers to be anti-parallel to it. According to the Pauli's principle, the second electron sharing the same molecular orbital should be anti-parallel to the first one. Thus, the electron which is close to the nucleus 2 prefers to be parallel to the nucleus 1. Finally, the dipole-dipole interaction between the second electron and nucleus 2 make the latter to be preferentially oriented anti-parallel to the nucleus 1. This effect is called *spin-spin coupling*, *J-coupling* or *scalar coupling*, because it is independent of the molecular orientation and on the strength of the external magnetic field.

The reasoning given above can in principle be extended to the other molecules and molecular fragments. Let us consider, for example, H-C-H fragment of the molecule, shown in Figure 4.3a. If we use the Hund's principle, telling that electrons occupying different but degenerate orbitals are parallel to each other, we find out that hydrogen nuclei tend to be parallel to each other. Analogously, in H-C-C-H fragment hydrogen nuclei tend to be anti-parallel (Figure 4.3b).

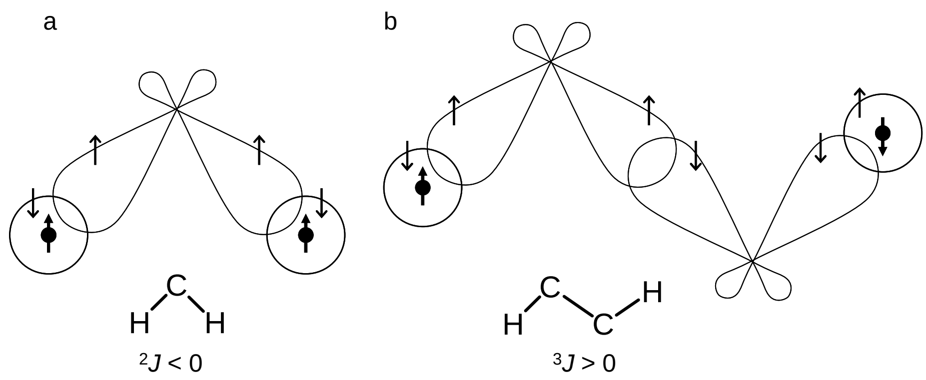

Figure 4.3. Scalar couplings in (a) H-C-H and (b) H-C-C-H molecular fragments.

In all cases the position of the energy level of the nucleus 2 depends on the spin state of nucleus 1.

4.2. Appearance of scalar coupling in NMR spectra.

Being much weaker then direct dipole-dipole interactions, scalar couplings are observable in the NMR spectra only when the dipole-dipole interactions are averaged out. This is usually the case for the relatively small molecules are studied in non-viscous medium. In this case scalar coupling appear as multiplet splittings of the spectral lines.

Before we procees, we have to define the following terms:

1) Nuclei are called chemically equivalent if they can be interchanged by a symmetry operation or a fast dynamical process. Chemical shifts of chemically equivalent nuclei are the same.

2) Chemically equivalent nuclei are called magnetically equivalent is they have the same scalar couplings to any of the spins in any other group of chemically equivalent spins.

Consider, for example, the nucleus A coupled with n nuclei X. Assume that nuclei A and X are chemically non-equivalent, while all X are chemically and magnetically equivalent. In the A part of the spectrum the number of the lines in the multiplet and their intensities are given by the number of the different energy levels of the X sub-system and their degeneracies, correspondingly. In practice, the structure of the multiplets is easy to determine using Pascal triangles, shown in Figure 4.4a for spins of X equal to 1/2 and in Figure 4.4b for spins of X equal to 1.

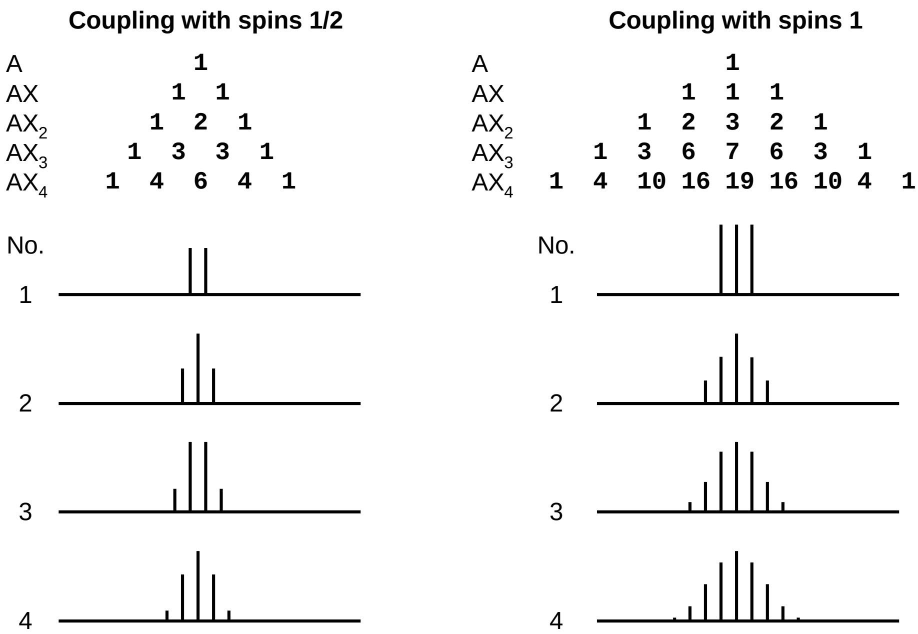

Figure 4.4. Splitting patterns for AX_n spin systems when n = 1-4. (a) Spin X equals to 1/2; (b) spin X equals to 1.

Scalar coupling constant is the distance between components of the multiplet, measured in Hz. Typical nomenclature for couplings is ${}^{m}J_{AX}$, where *m* stands for the number of bonds, separating A and X nuclei.

In case if the spin system contains more than two types of chemically non-equivalent nuclei, the overall splitting pattern can be constructed in the additive way. The example of this for the 3-spin system AMX is shown in Figure 4.5.

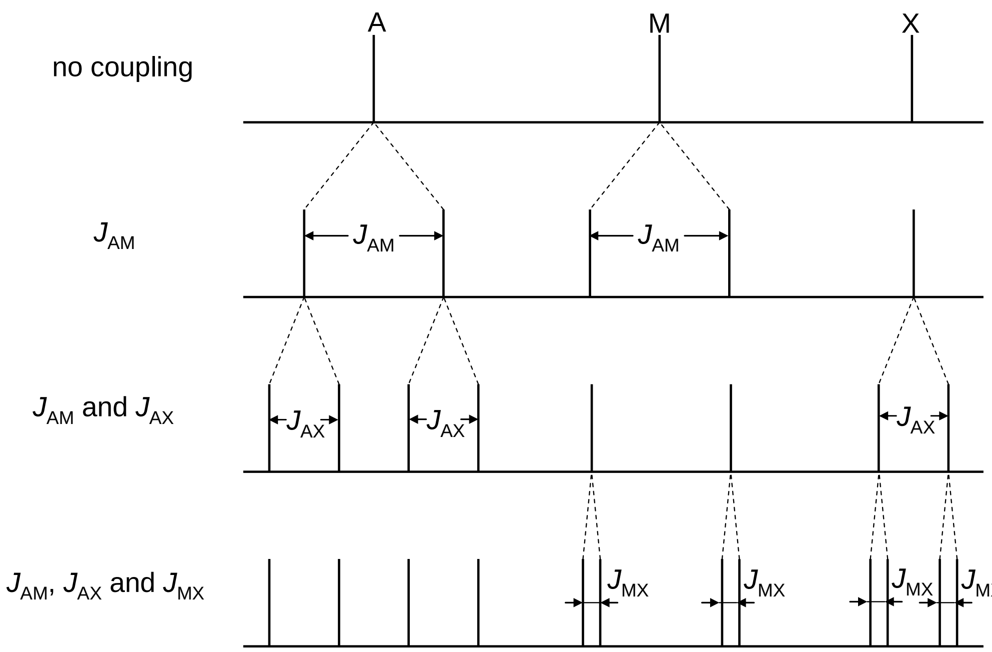

Figure 4.5. Splitting pattern for the AMX spin system. Assumption $J_{AM} > J_{AX} > J_{MX}$ was made.

The spectra shown above are called first-order spectra, which are valid if the scalar coupling constants are much smaller then the differences between resonance frequencies of coupled spins, i.e.

$$\left(\frac{J_{AX}}{\nu_A - \nu_X}\right)^2 << 1. \tag{4.1}$$

Otherwise, distortions of the multiplets may occur. The reason for the spectral distortion lies in the mixing of the spin wavefuncitons. Examples of the distortions are shown in Figures 4.6 and 4.7 for A_2X_2 and AX_3 spin systems, correspondingly.

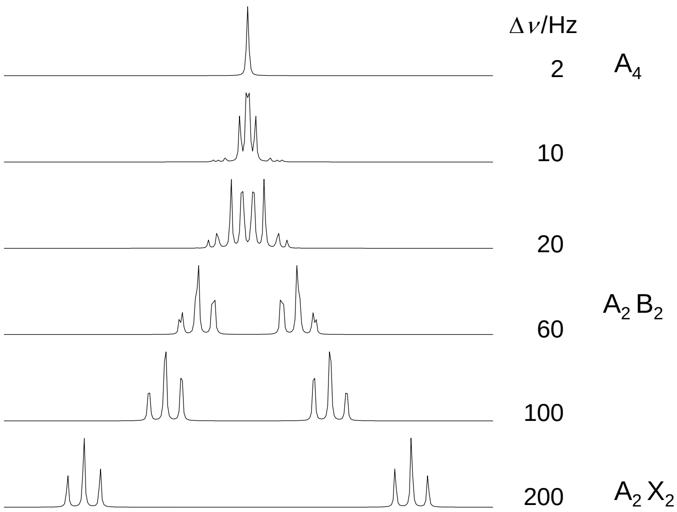

Figure 4.6. Transformations of the spectra of A_2X_2 spin system when resonance frequencies of A and X become closer. In the limit the system transforms into A_4 spin system.

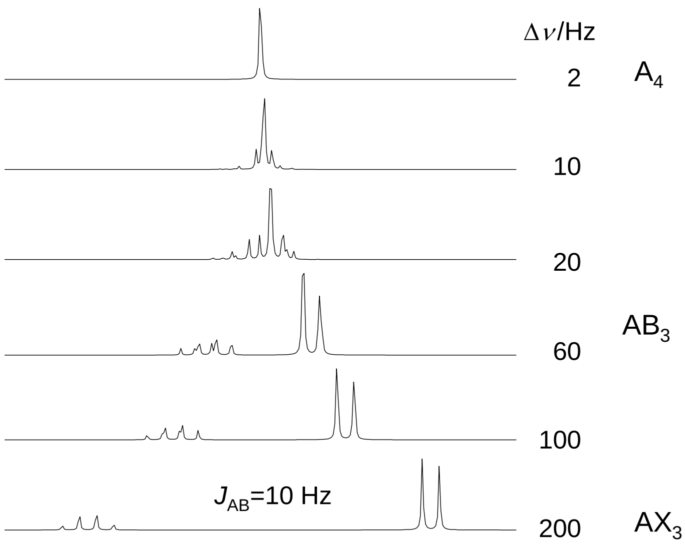

Figure 4.7. Transformations of the spectra of AX_3 spin system when resonance frequencies of A and X become closer. In the limit the system transforms into A_4 spin system.

4.3. Dependence of scalar coupling on molecular geometry.

The value of the scalar coupling depends of the electronic structure of the molecule. In particular, scalar coupling constants depend on the interatomic distances and angles. Few examples are given below.

In Figure 4.8 the CH distances in acetylene, ethylene and ethane are shown together with the values of the $^1J_{CH}$ coupling constants. It can be seen that the value of the coupling falls with increased CH distances. It can be anticipated that the oerall shape of the dependence in exponential.

≡C-H	=C-H	-C-H
(sp)	(sp^2)	(sp^3)
1.061 A in acetylene	1.085 A in ethylene	1.102 A in ethane
^2J = 250 Hz	^2J = 160 Hz	^2J = 130 Hz

Figure 4.8. CH distances and $^1J_{CH}$ scalar couplings in acetylene, ethylene and ethane.

In Figure 4.9a the dependence of the geminal $^2J_{HH}$ scalar coupling on the HCH angle is shown together with few examples. It can be seen that the wider is the angle, the smaller is the coupling.

In Figure 4.9b the dependence of the vicinal $^3J_{HH}$ scalar coupling on the dihedral HCCH angle is shown together with the typical equation, describing this dependence. The curve is known as Karplus diagram.

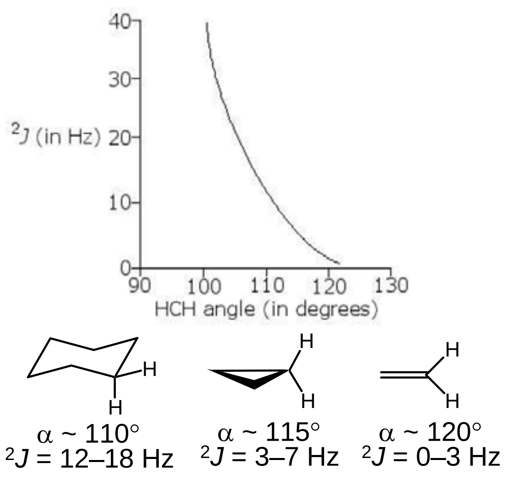

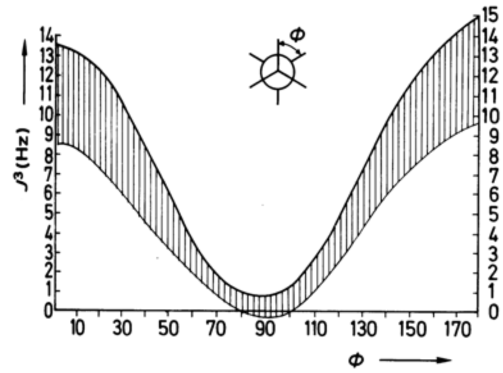

$$^3J = A\cos^2\Phi + B\cos\Phi + C$$

Figure 4.9. (a) The dependence of the geminal $^2J_{HH}$ scalar coupling on the HCH angle. (b) The dependence of the vicinal $^3J_{HH}$ scalar coupling on the dihedral HCCH angle.

4.4. Quantum-mechanical description of the scalar coupled two-spin system.

In order to find the spin energy levels E and the corresponding spin wavefunctions Ψ of the scalar coupled two-spin system one has to solve the Schrödinger equation

$$\hat{H}\Psi = E\Psi . \tag{4.2}$$

If we denote the first spin I and the second spin S, the spin Hamiltonian will be

$$\hat{H} = -\gamma_I B_0 \hat{I}_z - \gamma_S B_0 \hat{S}_z + \frac{2\pi}{\hbar} J \hat{\vec{I}} \cdot \hat{\vec{S}} , \tag{4.3}$$

where

$$\hat{\vec{I}} \cdot \hat{\vec{S}} = \hat{I}_x \hat{S}_x + \hat{I}_y \hat{S}_y + \hat{I}_z \hat{S}_z . \tag{4.4}$$

The first two terms in equation (4.3) are quantum-mechanical analogues of the classical expression (1.4) for the interaction energy of magnetic moment in magnetic field. The third term in (4.3) describes the scalar interaction, where J is the spin-spin coupling constant. J is conventionally expressed in Hz, which leads to the appearance of the conversion factor $\frac{2\pi}{\hbar}$ ..

Before we proceed with solving the Schrödinger equation, let us consider how do projections of the spin operator $\hat{I}_x$, $\hat{I}_y$ and $\hat{I}_z$ act of the spin wavefunctions $|\alpha\rangle$ and $|\beta\rangle$ (same expressions will be valid for $\hat{S}_x$, $\hat{S}_y$ and $\hat{S}_z$). It is possible to show that

$$\begin{array}{lll} \hat{I}_x|\alpha\rangle = +\frac{1}{2}\hbar|\beta\rangle & \hat{I}_y|\alpha\rangle = +\frac{i}{2}\hbar|\beta\rangle & \hat{I}_z|\alpha\rangle = +\frac{1}{2}\hbar|\alpha\rangle \\ \hat{I}_x|\beta\rangle = +\frac{1}{2}\hbar|\alpha\rangle & \hat{I}_y|\beta\rangle = -\frac{i}{2}\hbar|\alpha\rangle & \hat{I}_z|\beta\rangle = -\frac{1}{2}\hbar|\beta\rangle \end{array} \tag{4.5}$$

using the expressions (1.15)-(1.17) for the *z*-component and the postulate of quantum mechanics valid for any angular momentum operator:

$$\begin{aligned} \left[\hat{I}_x, \hat{I}_y\right] &= i\hbar\hat{I}_z \\ \left[\hat{I}_y, \hat{I}_z\right] &= i\hbar\hat{I}_x \\ \left[\hat{I}_z, \hat{I}_x\right] &= i\hbar\hat{I}_y \end{aligned} \tag{4.6}$$

For the system of two non-interacting spins wavefunctions are simply the products of the wavefunctions of individual spins (Zeeman products):

$$|\alpha\alpha\rangle \equiv 1, |\alpha\beta\rangle \equiv 2, |\beta\alpha\rangle \equiv 3, |\beta\beta\rangle \equiv 4 , \tag{4.7}$$

where the first letter describes spin I and the second letter describes spin S. Numbers 1, 2, 3 and 4 are introduced for simplicity. As operator $\hat{I}$ acts only on the first spin I and operator $\hat{S}$ acts only on the spin S, we obtain

$$\begin{array}{lll} \hat{I}_x|1\rangle = \hat{I}_x|\alpha\alpha\rangle = +\frac{1}{2}\hbar|\beta\alpha\rangle & \hat{I}_y|1\rangle = \hat{I}_y|\alpha\alpha\rangle = +\frac{i}{2}\hbar|\beta\alpha\rangle & \hat{I}_z|1\rangle = \hat{I}_z|\alpha\alpha\rangle = +\frac{1}{2}\hbar|\alpha\alpha\rangle \\ \hat{I}_x|2\rangle = \hat{I}_x|\alpha\beta\rangle = +\frac{1}{2}\hbar|\beta\beta\rangle & \hat{I}_y|2\rangle = \hat{I}_y|\alpha\beta\rangle = +\frac{i}{2}\hbar|\beta\beta\rangle & \hat{I}_z|2\rangle = \hat{I}_z|\alpha\beta\rangle = +\frac{1}{2}\hbar|\alpha\beta\rangle \\ \hat{I}_x|3\rangle = \hat{I}_x|\beta\alpha\rangle = +\frac{1}{2}\hbar|\alpha\alpha\rangle & \hat{I}_y|3\rangle = \hat{I}_y|\beta\alpha\rangle = -\frac{i}{2}\hbar|\alpha\alpha\rangle & \hat{I}_z|3\rangle = \hat{I}_z|\beta\alpha\rangle = -\frac{1}{2}\hbar|\beta\alpha\rangle \\ \hat{I}_x|4\rangle = \hat{I}_x|\beta\beta\rangle = +\frac{1}{2}\hbar|\alpha\beta\rangle & \hat{I}_y|4\rangle = \hat{I}_y|\beta\beta\rangle = -\frac{i}{2}\hbar|\alpha\beta\rangle & \hat{I}_z|4\rangle = \hat{I}_z|\beta\beta\rangle = -\frac{1}{2}\hbar|\beta\beta\rangle \end{array} \tag{4.8}$$

and

$$\begin{array}{lll} \hat{S}_x|1\rangle = \hat{S}_x|\alpha\alpha\rangle = +\frac{1}{2}\hbar|\alpha\beta\rangle & \hat{S}_y|1\rangle = \hat{S}_y|\alpha\alpha\rangle = +\frac{i}{2}\hbar|\alpha\beta\rangle & \hat{S}_z|1\rangle = \hat{S}_z|\alpha\alpha\rangle = +\frac{1}{2}\hbar|\alpha\alpha\rangle \\ \hat{S}_x|2\rangle = \hat{S}_x|\alpha\beta\rangle = +\frac{1}{2}\hbar|\alpha\alpha\rangle & \hat{S}_y|2\rangle = \hat{S}_y|\alpha\beta\rangle = -\frac{i}{2}\hbar|\alpha\alpha\rangle & \hat{S}_z|2\rangle = \hat{S}_z|\alpha\beta\rangle = -\frac{1}{2}\hbar|\alpha\beta\rangle \\ \hat{S}_x|3\rangle = \hat{S}_x|\beta\alpha\rangle = +\frac{1}{2}\hbar|\beta\beta\rangle & \hat{S}_y|3\rangle = \hat{S}_y|\beta\alpha\rangle = +\frac{i}{2}\hbar|\beta\beta\rangle & \hat{S}_z|3\rangle = \hat{S}_z|\beta\alpha\rangle = +\frac{1}{2}\hbar|\beta\alpha\rangle \\ \hat{S}_x|4\rangle = \hat{S}_x|\beta\beta\rangle = +\frac{1}{2}\hbar|\beta\alpha\rangle & \hat{S}_y|4\rangle = \hat{S}_y|\beta\beta\rangle = -\frac{i}{2}\hbar|\beta\alpha\rangle & \hat{S}_z|4\rangle = \hat{S}_z|\beta\beta\rangle = -\frac{1}{2}\hbar|\beta\beta\rangle \end{array} \tag{4.9}$$

If the spins can interact, the eigenfunctions of the Hamiltonian will no longer be Zeeman product functions (4.7). However, we can search for the new wavefunctions as linear combinations of the old ones:

$$\begin{aligned} \Psi_1 &= C_{11}|\alpha\alpha\rangle + C_{12}|\alpha\beta\rangle + C_{13}|\beta\alpha\rangle + C_{14}|\beta\beta\rangle \\ \Psi_2 &= C_{21}|\alpha\alpha\rangle + C_{22}|\alpha\beta\rangle + C_{23}|\beta\alpha\rangle + C_{24}|\beta\beta\rangle \\ \Psi_3 &= C_{31}|\alpha\alpha\rangle + C_{32}|\alpha\beta\rangle + C_{33}|\beta\alpha\rangle + C_{34}|\beta\beta\rangle \\ \Psi_4 &= C_{41}|\alpha\alpha\rangle + C_{42}|\alpha\beta\rangle + C_{43}|\beta\alpha\rangle + C_{44}|\beta\beta\rangle \end{aligned} \tag{4.10}$$

which can be shortened up to one expression

$$\Psi_i = \sum_{j=1}^{4} C_{ij}|j\rangle. \tag{4.11}$$

The matrix representation of the Hamiltonian (4.3) in the basis (4.7) is given by

$$\hat{H} = \begin{pmatrix} H_{11} & H_{12} & H_{13} & H_{14} \\ H_{21} & H_{22} & H_{23} & H_{24} \\ H_{31} & H_{32} & H_{33} & H_{34} \\ H_{41} & H_{42} & H_{43} & H_{44} \end{pmatrix}, \tag{4.12}$$

where

$$H_{ij} = \langle i|\hat{H}|j\rangle. \tag{4.13}$$

Let us find the explicit expression for the matrix elements (4.13).

$$H_{11} = \langle \alpha\alpha | \hat{H} | \alpha\alpha \rangle = \langle \alpha\alpha | -\gamma_I B_0 \hat{I}_z - \gamma_S B_0 \hat{S}_z + \frac{2\pi}{\hbar} J \hat{\vec{I}} \cdot \hat{\vec{S}} | \alpha\alpha \rangle = -\gamma_I B_0 \langle \alpha\alpha | \hat{I}_z | \alpha\alpha \rangle$$
$$- \gamma_S B_0 \langle \alpha\alpha | \hat{S}_z | \alpha\alpha \rangle + \frac{2\pi}{\hbar} J \left(\langle \alpha\alpha | \hat{I}_x \hat{S}_x | \alpha\alpha \rangle + \langle \alpha\alpha | \hat{I}_y \hat{S}_y | \alpha\alpha \rangle + \langle \alpha\alpha | \hat{I}_z \hat{S}_z | \alpha\alpha \rangle \right) \tag{4.14}$$

Using (4.8) and (4.9) we obtain

$$H_{11} = -\gamma_I B_0 \frac{\hbar}{2} \langle \alpha\alpha \| \alpha\alpha \rangle - \gamma_S B_0 \frac{\hbar}{2} \langle \alpha\alpha \| \alpha\alpha \rangle +$$
$$\frac{2\pi}{\hbar} J \left(\frac{\hbar}{2} \langle \alpha\alpha | \hat{I}_x | \alpha\beta \rangle + \frac{i\hbar}{2} \langle \alpha\alpha | \hat{I}_y | \alpha\beta \rangle + \frac{\hbar}{2} \langle \alpha\alpha | \hat{I}_z | \alpha\alpha \rangle \right) =$$
$$-\gamma_I B_0 \frac{\hbar}{2} - \gamma_S B_0 \frac{\hbar}{2} + \frac{2\pi}{\hbar} J \left(\frac{\hbar}{2} \frac{\hbar}{2} \langle \alpha\alpha \| \beta\beta \rangle + \frac{i\hbar}{2} \frac{i\hbar}{2} \langle \alpha\alpha \| \beta\beta \rangle + \frac{\hbar}{2} \frac{\hbar}{2} \langle \alpha\alpha \| \alpha\alpha \rangle \right) =$$
$$-\gamma_I B_0 \frac{\hbar}{2} - \gamma_S B_0 \frac{\hbar}{2} + \frac{2\pi}{\hbar} J \frac{\hbar^2}{4} = -\omega_I \frac{\hbar}{2} - \omega_S \frac{\hbar}{2} + \frac{2\pi\hbar}{4} J \tag{4.15}$$

Here, we have used the orhtogonality of the Zeeman product states. Substituting $\hbar\omega$ with $h\nu$ and expressing the matrix element in frequency units we get

$$H_{11} = -\frac{\nu_I}{2} - \frac{\nu_S}{2} + \frac{J}{4} \tag{4.16}$$

After performing the analogous calculations for the other matrix elements of the Hamiltonian the following matrix is constructed:

$$\hat{H} = \begin{pmatrix} -\frac{\nu_I}{2} - \frac{\nu_S}{2} + \frac{J}{4} & 0 & 0 & 0 \\ 0 & -\frac{\nu_I}{2} + \frac{\nu_S}{2} - \frac{J}{4} & \frac{J}{2} & 0 \\ 0 & \frac{J}{2} & +\frac{\nu_I}{2} - \frac{\nu_S}{2} - \frac{J}{4} & 0 \\ 0 & 0 & 0 & +\frac{\nu_I}{2} + \frac{\nu_S}{2} + \frac{J}{4} \end{pmatrix}. \tag{4.17}$$

All off-diagonal elements appeared to be zero, apart of H_{23} and H_{32}, which describe the mixing of the spin states $|\alpha\beta\rangle$ and $|\beta\alpha\rangle$, as it will become clear later. The new energy levels are the eigenvalues of the matrix (4.17), which can be found as solutions of the following polynomial equation:

$$\begin{vmatrix} -\frac{\nu_I}{2}-\frac{\nu_S}{2}+\frac{J}{4}-E & 0 & 0 & 0 \\ 0 & -\frac{\nu_I}{2}+\frac{\nu_S}{2}-\frac{J}{4}-E & \frac{J}{2} & 0 \\ 0 & \frac{J}{2} & +\frac{\nu_I}{2}-\frac{\nu_S}{2}-\frac{J}{4}-E & 0 \\ 0 & 0 & 0 & +\frac{\nu_I}{2}+\frac{\nu_S}{2}+\frac{J}{4}-E \end{vmatrix}=0\,. \quad (4.18)$$

Two solutions are obvious:

$$\begin{aligned} E_1 &= -\frac{\nu_I}{2}-\frac{\nu_S}{2}+\frac{J}{4} \\ E_4 &= +\frac{\nu_I}{2}+\frac{\nu_S}{2}+\frac{J}{4} \end{aligned} \quad (4.19)$$

Two other solutions can be found as the determinant

$$\begin{vmatrix} -\frac{\nu_I}{2}+\frac{\nu_S}{2}-\frac{J}{4}-E & \frac{J}{2} \\ \frac{J}{2} & +\frac{\nu_I}{2}-\frac{\nu_S}{2}-\frac{J}{4}-E \end{vmatrix}=0\,, \quad (4.20)$$

which gives

$$\left(-\frac{\nu_I}{2}+\frac{\nu_S}{2}-\frac{J}{4}-E\right)\left(\frac{\nu_I}{2}-\frac{\nu_S}{2}-\frac{J}{4}-E\right)-\frac{J^2}{4}=0\,. \quad (4.21)$$

Quadratic equation (4.21) has solutions:

$$E_{2,3}=\mp\frac{1}{2}\sqrt{(\nu_I-\nu_S)^2+J^2}-\frac{J}{4}\,. \quad (4.22)$$

It is convenient to introduce the parameter, which describes the deviation of the scalar-coupled two-spin system from the system of two non-interacting spins:

$$Q=\left(\frac{J}{\nu_I-\nu_S}\right)^2. \quad (4.23)$$

Thus, equation (4.22) can be rewritten as

$$E_{2,3}=\mp\frac{1}{2}(\nu_I-\nu_S)\sqrt{1+Q}-\frac{J}{4}\,. \quad (4.24)$$

Let us consider two limiting cases: a) $Q=0$ and b) $Q\to\infty$.

a) $Q = 0$, i.e. the scalar coupling is much smaller than the difference between resonance frequencies of spins I and S: $|J| << |\nu_I - \nu_S|$. This would be the case of AX spin system with heteronuclear scalar coupling, or the homonuclear scalar coupling is the signals are distant in the spectrum. We get

$$E_2 = -\frac{\nu_I}{2} + \frac{\nu_S}{2} - \frac{J}{4}$$
$$E_3 = +\frac{\nu_I}{2} - \frac{\nu_S}{2} - \frac{J}{4} \qquad (4.25)$$

b) $Q \to \infty$, i.e. the scalar coupling is much bigger than the difference between resonance frequencies of spins I and S: $|J| >> |\nu_I - \nu_S|$. This is the limiting case A_2 spin system with the scalar coupling between chemically equivalent nuclei. We get

$$E_2 = -\frac{3}{4}J$$
$$E_3 = +\frac{1}{4}J \qquad (4.26)$$

In intermediate cases, when $|J|$ and $|\nu_I - \nu_S|$ are comparable, the spin system is described as AB. The energy level diagrams for the A+X, AX, AB and A_2 spin systems are shown in Figure 4.10

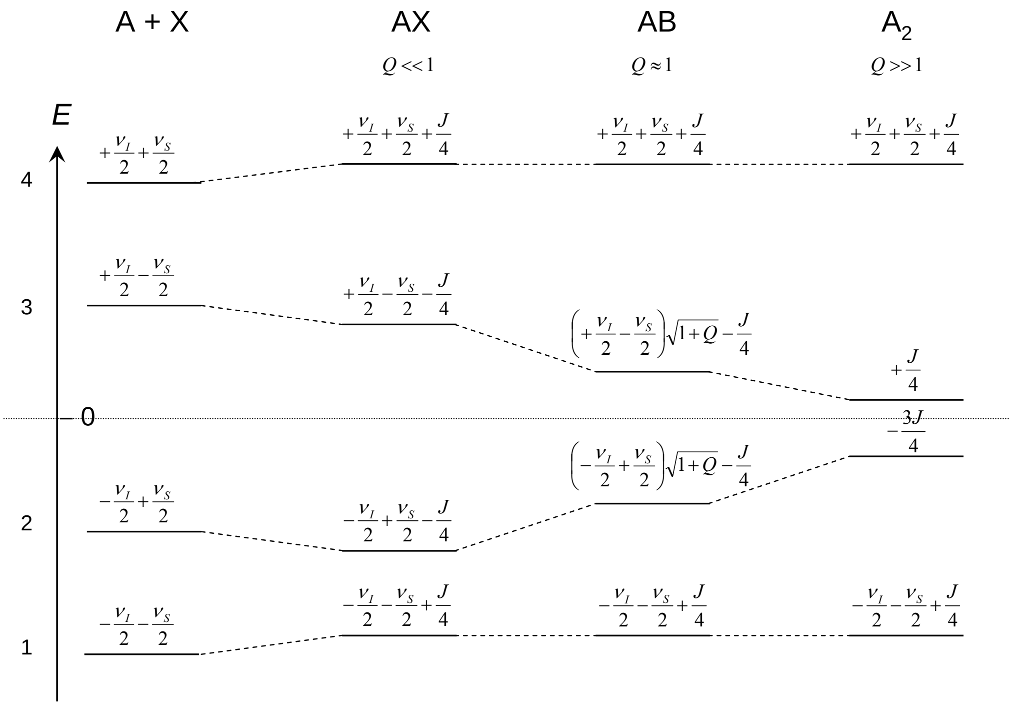

Figure 4.10. Energy level diagrams for the scalar coupled A+X, AX, AB and A_2 two-spin systems.

For each spin system the four wavefunctions, corresponding to the four energy levels, can be found by solving the equation (4.2) with Hamiltonian (4.17) and the corresponding value of energy, taken from (4.19) or (4.22). In other words, for each E_i, where $i = 1,2,3,4$ one has to solve the system of four linear equations. The result gives the set of coefficients C_{ij} ($j = 1,2,3,4$) for the linear combinations (4.10). It can be demonstrated that

$$\begin{aligned}
\Psi_1 &= 1|\alpha\alpha\rangle + 0|\alpha\beta\rangle + 0|\beta\alpha\rangle + 0|\beta\beta\rangle \\
\Psi_2 &= 0|\alpha\alpha\rangle + C_{22}|\alpha\beta\rangle + C_{23}|\beta\alpha\rangle + 0|\beta\beta\rangle \\
\Psi_3 &= 0|\alpha\alpha\rangle + C_{32}|\alpha\beta\rangle + C_{33}|\beta\alpha\rangle + 0|\beta\beta\rangle \\
\Psi_4 &= 0|\alpha\alpha\rangle + 0|\alpha\beta\rangle + 0|\beta\alpha\rangle + 1|\beta\beta\rangle
\end{aligned} \tag{4.27}$$

or

$$\begin{aligned}
\Psi_1 &= |\alpha\alpha\rangle \\
\Psi_2 &= C_{22}|\alpha\beta\rangle + C_{23}|\beta\alpha\rangle \\
\Psi_3 &= C_{32}|\alpha\beta\rangle + C_{33}|\beta\alpha\rangle \\
\Psi_4 &= |\beta\beta\rangle
\end{aligned} \tag{4.28}$$

where

$$\begin{aligned}
&C_{22} = C_{33} = \sqrt{\frac{1}{2} + \frac{1}{2\sqrt{1+Q}}} \text{ and} \\
&C_{23} = -C_{32} = -\frac{1}{2C_{22}\sqrt{1+\frac{1}{Q}}}.
\end{aligned} \tag{4.29}$$

The wavefunctions (4.28) are normalized:

$$\begin{aligned}
&C_{22}^{\ 2} + C_{23}^{\ 2} = 1 \text{ and} \\
&C_{32}^{\ 2} + C_{33}^{\ 2} = 1.
\end{aligned} \tag{4.30}$$

Again, we consider two limiting cases:

a) $Q = 0$ (AX spin system)

$$C_{22} = C_{33} = 1 \text{ and } C_{23} = C_{32} = 0, \tag{4.31}$$

thus we get

$$\begin{aligned}
\Psi_2 &= |\alpha\beta\rangle \\
\Psi_3 &= |\beta\alpha\rangle
\end{aligned} \tag{4.32}$$

The functions coincide with the Zeeman product states.

b) $Q \to \infty$ (A_2 spin system).

$$C_{22} = C_{33} = \frac{1}{\sqrt{2}} \text{ and } C_{23} = C_{32} = -\frac{1}{\sqrt{2}}, \tag{4.33}$$

thus we get

$$\begin{aligned} \Psi_2 &= \frac{1}{\sqrt{2}}\left(\left|\alpha\beta\right\rangle - \left|\beta\alpha\right\rangle\right) \\ \Psi_3 &= \frac{1}{\sqrt{2}}\left(\left|\alpha\beta\right\rangle + \left|\beta\alpha\right\rangle\right) \end{aligned} \tag{4.34}$$

The functions $\left|\alpha\beta\right\rangle$ and $\left|\beta\alpha\right\rangle$ are completely mixed.

In intermediate cases, when $Q \approx 1$ the wavefunctions $\left|\alpha\beta\right\rangle$ and $\left|\beta\alpha\right\rangle$ to be mixed only to a certain degree, intermediate between (4.32) and (4.34). The wavefunctions for the scalar coupled A+X, AX, AB and A_2 spin systems are shown in Figure 4.11.

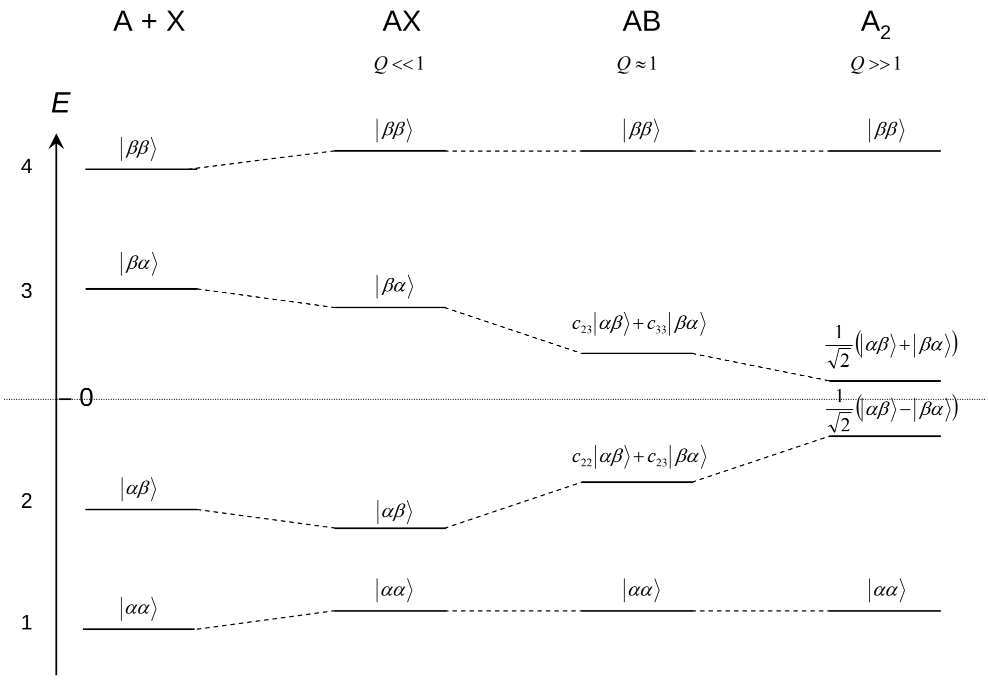

Figure 4.11. Spin wavefunctions for the scalar coupled A+X, AX, AB and A_2 two-spin systems.

Having the wavefunctions established, we can calculate the probabilities of the transitions between energy levels, which are proportional to the signal intensities in the NMR spectrum. Transitions of the spin I are $1 \to 3$ and $2 \to 4$, while transitions of spin S are $1 \to 2$ and $3 \to 4$. In the time-dependent perturbation theory it is shown that probability of transition between states $\left\langle initial\right|$ and $\left|final\right\rangle$ under the influence of the perturbation $\hat{H}'$ is given by

$$Intensity \propto \left(\left\langle initial\right|\hat{H}'\left|final\right\rangle\right)^2. \tag{4.35}$$

In case of NMR transitions the perturbation operator describes the interaction of the nuclear magnetic moments with the magnetic field of the pulse. The latter is polarized in the horizontal plane, so for simplicity we can consider only the *x*-compoment of the field. Assuming the homonuclear scalar coupling and skipping the constant factors we obtain

$$Intensity \propto \left(\left\langle initial\left|\hat{I}_x + \hat{S}_x\right| final\right\rangle\right)^2 . \tag{4.36}$$

Let us consider for example transition $1 \to 3$.

$$\begin{aligned}
&Intensity_{13} \propto \left(\left\langle \alpha\alpha\left|\hat{I}_x + \hat{S}_x\right| C_{32}\alpha\beta + C_{33}\beta\alpha\right\rangle\right)^2 = \\
&\left(C_{32}\left\langle \alpha\alpha\left|\hat{I}_x + \hat{S}_x\right|\alpha\beta\right\rangle + C_{33}\left\langle \alpha\alpha\left|\hat{I}_x + \hat{S}_x\right|\beta\alpha\right\rangle\right)^2 = \\
&\left(C_{32}\left\langle \alpha\alpha\left|\hat{I}_x\right|\alpha\beta\right\rangle + C_{32}\left\langle \alpha\alpha\left|\hat{S}_x\right|\alpha\beta\right\rangle + C_{33}\left\langle \alpha\alpha\left|\hat{I}_x\right|\beta\alpha\right\rangle + C_{33}\left\langle \alpha\alpha\left|\hat{S}_x\right|\beta\alpha\right\rangle\right)^2 = . \\
&\left(C_{32}\frac{\hbar}{2}\left\langle \alpha\alpha \| \beta\beta\right\rangle + C_{32}\frac{\hbar}{2}\left\langle \alpha\alpha \| \alpha\alpha\right\rangle + C_{33}\frac{\hbar}{2}\left\langle \alpha\alpha \| \alpha\alpha\right\rangle + C_{33}\frac{\hbar}{2}\left\langle \alpha\alpha \| \beta\beta\right\rangle\right)^2 = \\
&\frac{\hbar^2}{4}\left(C_{32} + C_{33}\right)^2
\end{aligned} \tag{4.37}$$

Using (4.29) and (4.30) we get

$$Intensity_{13} \propto= \frac{\hbar^2}{4}\left(1 + 2C_{32}C_{33}\right) = \frac{\hbar^2}{4}\left(1 + \sqrt{\frac{Q}{Q+1}}\right) = \frac{\hbar^2}{4}\left(1 + f\right), \tag{4.38}$$

where

$$f = \sqrt{\frac{Q}{Q+1}} . \tag{4.39}$$

The allowed transitions and the corresponding spectral lines for the scalar coupled A+X, AX, AB and A_2 spin systems are shown in Figure 4.12.

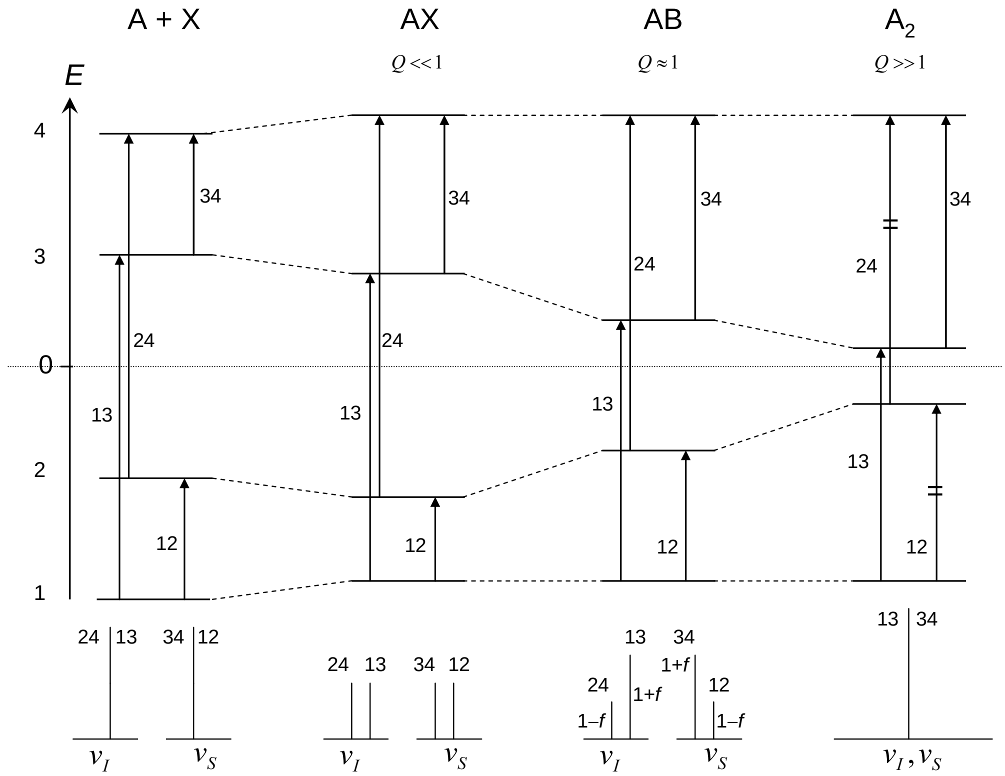

Figure 4.12. Allowed transitions and corresponding spectral lines for the scalar coupled A+X, AX, AB and A_2 two-spin systems.

The Figure (4.12) can be rationalized as follows. Two non-coupled spins (A+X) will give two singlets in the NMR spectrum. Weak scalar coupling (AX) will lead to the splitting of the lines into doublet. Components of the doublets are separated by the value of the scalar coupling constant J and have equal intensities. If the scalar coupling constant is comparable with the distance between signals measured in Hz (AB), the doublets are distorted by so called *roof effect*: inner components of the multiplets are more intensive that the outer ones (inner components "borrow" the intensity from the outer ones). Finally, in the A2 spin system transitions $1 \rightarrow 2$ and $2 \rightarrow 4$ are forbidden, while the other two, $1 \rightarrow 3$ and $3 \rightarrow 4$ have identical frequency and thus in the resulting spectrum only one line appears. This explains why we do not see scalar spin-spin couplings between chemically equivalent nuclei, such as three protons in CH_3 group.